FACULTY OF TECHNOLOGY

Cellulose-based templating agents in the production of novel mesoporous geopolymer-based heterogeneous catalysts

Arafat Hossain

Master's Degree Programme in Energy and Environmental Engineering

Master's thesis

December 2020

ABSTRACT

Title of the thesis		Research Group
Cellulose-based templating agents in the production of novel mesoporous geopolymer-based heterogeneous catalysts		Fibre and Particle Engineering
Author	**Thesis Supervisor**	
Arafat Hossain	Dr. Mohammad Al-Zeer; Dr. Satu Ojala	
Degree Program	**Thesis type**	**Number of pages**
Energy and Environmental Engineering, University of Oulu	Master's thesis	83pages +1appendix(7pages)
Submission date		
14.01.2021		

Abstract

This thesis examines the novel approach of synthesizing mesoporous geopolymer by hard templating technique using cellulose nanocrystals (CNCs) as the templating agent. Geopolymers have the advantage of tailoring their porosity to form hierarchical porous structure which makes them a promising material in the field of heterogeneous catalysis. Hard templating technique is one of the options through which the porosity of the geopolymer can be tailored in more controllable manner compared to post-synthetic treatment approaches. Thus synthesizing geopolymer through hard templating technique using CNCs as template has the potential of producing mesoporous geopolymer with high surface area and high pore volume which was the prime objective of this thesis. Moreover, the synthesized geopolymer-CNC composites are also environmental friendly and cost-effective as the raw materials for geopolymers are obtained from naturally occurring materials and CNCs are obtained mainly from the trees and plants which also make them abundantly available.

This study presents the synthesis and characteristics of the synthesized geopolymer- CNC composites and investigates the reasons for not having the desired surface area and pore volume in any of the samples. A number of trials were made in the whole work by modifying the chemical composition of geopolymer-CNC composites and also by modifying the synthesis procedure. In all the trials, the molar ratio for SiO_2/Al_2O_3 for normal geopolymer was ~3.5 and for the one synthesized with high silicon content was ~6.5. Different weight percentage of CNCs was added to geopolymer in different attempt of this work. Two forms of CNC were applied; one was aqueous suspension form used as received from the supplier and another was freeze dried form. CNC template was removed from the geopolymer by calcination in air. Ion-exchange of the calcined powder was performed to generate the acidic sites into the geopolymer framework. To induce secondary mesoporosity into geopolymer structure acid wash followed by ion-exchange was also performed in one of the trials.

As the main goal of this work to synthesize mesoporous geopolymer with high surface area and pore volume, most of prepared samples underwent only N_2 adsorption-desorption technique in most of the trials. Because of the low surface area and pore volume, only the samples prepared in the final attempt of this thesis underwent further analysis through XRD, FT-IR spectrometry, Raman spectrometry, TGA-MS, SEM, TEM alongside N_2 adsorption-desorption technique to investigate the reason for not getting the desired outcome. From the obtained results of different analysis, some promising results were found from the SEM micrographs of the geopolymer that was prepared with 10wt% aqueous suspension of CNCs and cured at 40° C overnight. Round shaped elements were found which were well dispersed on the geopolymer surface. These elements were assumed to be rod-shaped cellulose nanocrystals which were embedded in the geopolymer particles. The presence of these elements was found even in the samples that were thermally treated at 650° C for longer period of times.

Assuming the obtained particles in geopolymer matrix are CNCs, some modifications can be made in the future endeavors which may include acid hydrolysis of the geopolymer-CNC composite to decompose cellulose nanocrystals or thermal decomposition at a different temperature with different heating rate. If decomposed successfully, the

synthesized mesoporous geopolymer may contain promising potential to be used in various heterogeneous catalysis applications.

Keywords: Heterogeneous catalysis, Geopolymer, Cellulose nanocrystals, Hard templating

FOREWORD

The purpose of this thesis involves a novel approach to induce mesoporosity into geopolymer to use them as potential heterogeneous catalyst using cellulose nanocrystals as hard templates. The work was performed at University of Oulu, in Fibre and Particle Engineering laboratory.

I am grateful to the Almighty for his endless blessings and mercy. I want to express my sincere gratitude to Prof. Mirja Illikainen for considering me worthy to work in the Fibre and Particle Engineering research group. To my supervisor Dr. Mohammad Al-Zeer, I am immensely thankful for his countless support, for the guidance and for being a great mentor throughout my whole thesis journey. I also want to thank my secondary supervisor Dr. Satu Ojala for her precious contribution during my entire endeavor.

I want to thank all our Laborants Jarno, Jani and Elisa for their assistance and valuable instructions during my work. I am also grateful to the other researchers of Fibre and Particle Engineering research group for their kind assistance throughout my entire work. My sincere appreciation also goes to all the technicians involved in conducting different characterization techniques during different phases of my work.

In the concluding part, I want to thank my parents and my siblings from my heart for their love, affection and moral support throughout my entire journey. I also want to acknowledge the love and contribution of my other family members.

Oulu, 13.01.2021

Arafat Hossain
Author

TABLE OF CONTENTS

LIST OF ABBREVIATIONS

ZIFs	Zeolitic Imidazolate Frameworks
MOFs	Metal-Organic Frameworks
FCC	Fluid Catalytic Cracking
HC	Hydro Cracking
nm	nanometer
μm	micrometer
IUPAC	International Union for Pure and Applied Chemistry
SDAs	Structural Directing Agents
TLCT	True Liquid Crystal Templating
CNT	Carbon Nanotubes
CVD	Chemical Vapor Deposition
NCs	Nano-Celluloses
CNCs	Cellulose Nanocrystals
HPC	Hydroxypropylcellulose
EC	Ethylcellulose
TMOS	Tetramethoxysilane
EISA	Evaporation Induced Self-Assembly
OPC	Ordinary Portland Cement
CTAB	Cetyl Trimethylammonium Bromide
UV	Ultra-Violet
XRD	X-ray Diffraction
TGA	Thermogravimetric Analysis
SEM	Scanning Electron Microscopy
TEM	Transmission Electron Microscopy
FTIR	Fourier Transform Infrared Spectroscopy
Na_2H_2EDTA	Ethylenediaminetetraacetic acid
FD	Freeze dried

1 INTRODUCTION

1.1 Background

Heterogeneous catalysis holds immense potential to boost the World's economy by converting the raw materials into desired chemicals and fuels in economic, efficient and environmentally friendly manner. Heterogeneous catalysis is widely used in many industrial processes such as food, pharmaceutical and petrochemical industries. It's been stated that almost 90% of all chemical processes use heterogeneous catalysis (Dumesic et al., 2008). In heterogeneous catalysis, catalysts are in different physical phase from the reactants and the products. Typical heterogeneous catalysts are mostly inorganic solids e.g. metals, metal salts, oxides and sulphides. But sometimes organic materials like organic hydroperoxides (Deutschmann et al., 2011), metal-organic frameworks (MOFs) derived solid bases (Zhu et al., 2017), zeolitic imidazolate frameworks (ZIFs) (Horiuchi et al., 2015) can also act as heterogeneous catalyst. As the catalysts and the reactants are in different forms, heterogeneous catalysis provides the advantage of easily being separated from the reaction mixtures. The separation technique is also straightforward and cheaper (e.g. filtration). After the separation, solid catalysts can be used again. This characteristic makes heterogeneous catalysis an attractive choice for numerous chemical processes.

Solid catalysts are often porous materials. Of all the solids catalysts available, zeolites are the most extensively applied in various industrially significant chemical reactions.

Zeolites are three-dimensional, crystalline, inorganic solids consisting mainly of silicon, aluminium and oxygen in their framework that contains cavities and channels of specific molecular dimensions (0.3–1.5 nm diameter). The zeolites structure is composed of SiO_4 and AlO_4^- tetrahedral units which are connected with each other through their common oxygen atom to create open microporous framework. These tetrahedral units are connected to each other by their corners and may generate the shape of linked cages, cavities or channels. These cavities or channels hold enough space that can be occupied by large ions or water molecules which may have sufficient freedom to drift freely into and out of the structure leaving free space for guest molecules of specific size, shape and

polarity. This is termed as molecular sieving effect of zeolites. (Li et al., 2017) This also leads to the path of ion-exchange and reversible dehydration. (Dyer, 2001; Martínez and Corma, 2013). The tetrahedrally coordinated aluminium atoms carry negative charge in the zeolite framework which is compensated by charge-balancing cations in extra framework positions. These cations are mostly located in several different sites throughout the pores and cavities of zeolite. These cations can be either inorganic or organic. The original ones present in the as-synthesized sample can be replaced by others which gives zeolite ion-exchange capacity (Martínez and Corma, 2013). Through ion-exchange with ammonium solutions or rare earth salts different acidic sites (Brønsted or Lewis) can be generated in zeolite framework (Humphries et al., 1993). These acidic sites in the zeolite framework combine with the microporous network offer zeolites a unique privilege of undergoing shape-selective catalysis for the formation of specific products. High hydrothermal stability, low production costs along with the mentioned characteristics of zeolites made them widely used as detergents, adsorbents, and highly efficient catalyst in numerous chemical processes. To be specific, the potential of zeolites as heterogeneous catalyst made them highly attractive in oil refining and petrochemical industries for producing large amount of gasoline from crude oil through fluid catalytic cracking (FCC) and hydro cracking (HC) (Li et al., 2017; Weckhuysen and Yu, 2015). Other applications of zeolites include soil conditioners, nutrient release agents in horticulture, remover of radio-active isotope from waste water (Weckhuysen and Yu, 2015). However, despite their significance in chemical processes, zeolites still suffer from the limitation of having strict micro porosity (normally <1.2 nm) which deters them from being used in liquid phase systems especially with bulk molecules. Because of their microporous structure, larger molecules cannot diffuse through the pores which results in the deactivation of the catalyst and shortens their lifetime. (Alzeer et al., 2017)

Overcoming this limitation resulted in the development of various porous catalysts with well-defined pores at different length scales. International Union of Pure and Applied Chemistry (IUPAC) has classified these pores into 3 categories depending on the width of the pores: Macropores (> 50 nm), Mesopores (2-50nm) and Micropores (<2 nm) (Sing, 1991).

1.2 Synthesis of porous material

Synthesis of desired porous materials is commonly achieved through the application of structural directing agents (SDAs). For applying SDAs to the guest materials two synthesis pathways are generally followed: 1) Soft templating 2) Hard templating or nanocasting.

1.2.1 Soft Templating

Soft templating technique focuses on combining surfactant molecules with a suitable guest species to form ordered mesoporous structure which is obtained after the removal of the templating agent. Homogeneous clear solution of surfactants is required in order to obtain the desired structure. This ordered mesostructure mainly can be achieved through two different synthetic strategies in this particular pathway: one is cooperative self-assembly and another is "true" liquid-crystal templating (TLCT) process as shown in Figure 1 (Marcos-Hernández and Villagrán, 2019).

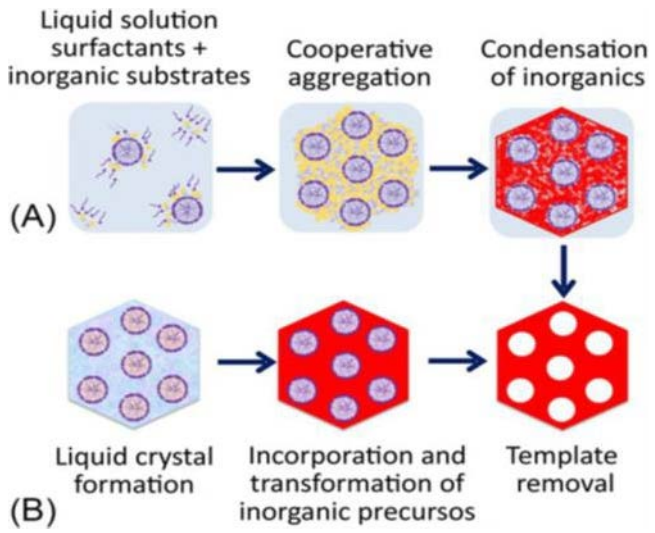

Figure 1. Representation of the two soft-templating scheme: (A) cooperative self-assembly (B) "true" liquid-crystal templating process for the synthesis of ordered mesoporous material. Reproduced with the permission from Marcos-Hernández and Villagrán (2019).

In cooperative self-assembly process, the interaction between inorganic species and the surfactants may take place through covalent bonds, electrostatic forces or hydrogen

bonding. The polymerization or cross-linking which eventually result in the assembly of inorganic species and surfactants occurs usually at the interface. The order of arrangement of the surfactants is largely influenced by the charge density of the two species. Due to this charge density, the composition of the inorganic/organic hybrids seems to differ to some extent. Hence, matching between the charge density at the interface largely govern the self-assembly. The final mesophase that is obtained through the cooperative self-assembly process is the ordered 3D arrangement with the lowest interface energy. In a different approach, in the "true" liquid crystal templating process, surfactant molecules are transformed into semi-liquid or true crystalline mesophase micelles from which templates are formed. When the inorganic precursors are incorporated to the template, they grow in the confined space around the surfactants and then condenses. This confined growth contributes to the enhanced condensation of the inorganic precursors and ceramic like frameworks are formed. After the condensation, the organic template is removed either by calcination or extraction and eventually the mesostructures along with pore sizes and symmetries are casted from liquid-crystal scaffolds. (Marcos-Hernández and Villagrán, 2019; Wan and Zhao, 2007)

Soft templating often includes the application of either cationic, anionic, non-ionic surfactants or sometimes mixed surfactants with a view to control the order of the pore structures along with pore architectures. Some of the reported commonly used cationic surfactants are alkyltrimethyl quaternary ammonium surfactant, gemini surfactants, bolaform surfactants, multiheadgroup surfactants, cationic fluorinated surfactants. (Wan and Zhao, 2007)

However, soft templating method contains few disadvantages. One notable demerit of using soft templates is that they are hard to predict because of the dynamic nature of numerous soft-templating systems which makes them difficult to understand and characterize time to time. Most of the time the demerits emerged from soft templating can be unraveled through adopting "hard templating" approach.

1.2.2 Hard Templating

Hard templating method is also known as "nanocasting" and is another method to induce mesoporosity into specific materials. Hard templating involves using a rigid, preformed

template which is made from aggregates of nanoparticles. This template is filled or covered with precursor materials and then the precursor materials is treated to form the target material within the template. After the formation of the desired material, the template is removed to generate a replica. The main difference between soft and hard templating is for soft templating the cooperative assembly between the surfactant and inorganic phase is always a prerequisite while hard templating approach makes only the replica of the surfactant of certain structure. Because of the preformed structure of the hard templates, hard templating contributes to the better control of the pore structure of the precursor materials. In addition, most hard templates contain rigid structure and these rigid structures are capable of exhibiting greater resistance towards the high temperature. So, it is also possible to generate highly crystalline or single crystal materials through hard templating. (Marcos-Hernández and Villagrán, 2019; Yang et al., 2015)

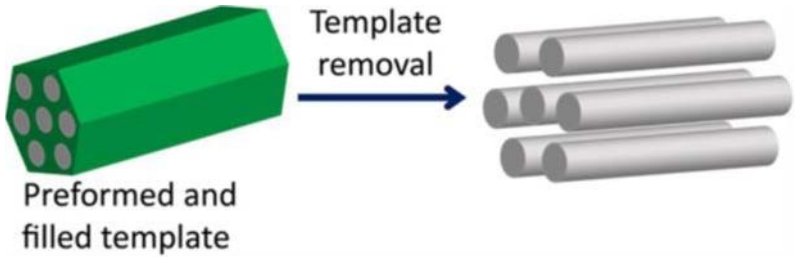

Figure 2. Representation of Hard-templating scheme through the addition of precursor material into the previously formed template and template removal. Reproduced with the permission from Marcos-Hernández and Villagrán (2019).

There is a wide range of templates available for hard templating purpose. Of them, porous membrane, polymer microspheres, plastic foam, porous anodic aluminium oxide are the most common (Xie et al., 2016). Some recent attempts have included carbon based materials for hard templating because of their abundancy in nature and low cost. Because of the potential to be used as both physical and chemical template, carbon nanotubes (CNT) can be used to fabricate materials that inherits the morphology with 1-dimensional rod or tube like shape (Zhu et al., 2012). The significance of CNTs is that it can act either as a scaffold or chemical reagent in the synthesis of metal carbides and nitrides. Dai and Lieber reported first the development of a Chemical Vapor Deposition (CVD) method for the synthesis of metal carbide using CNTs as reagent and also as hard template (Dai et

al., 1995). A series of nanorods (TiC, NbC, Fe_3C, SiC, BCx) can be synthesized through this method (Zhu et al., 2012).

Of all the biopolymers existing on earth, cellulose has been found to be most abundant and most of the cellulose derivatives have good potential to be used in advanced chemical applications. Cellulose are mainly found in trees, bacteria, plants and fungi. It's been reported that around 90 billion metric tons of cellulose fibres are produced per annum worldwide (Pinkert et al., 2009). Nanocelluloses (NCs) can be obtained by the degradation of cellulose fibres. There are different forms of NCs available and of them, cellulose nanocrystals (CNCs) and cellulose nanofibers (CNFs) are the most common because of their relatively easy extracting method from the raw cellulose material. However, because of their interesting chemical structure, CNCs have been reported to be adopted in many advanced materials applications in recent years (e.g. templating). In addition, CNCs are cheaper (<$50 per kg) than frequently used carbon material templating agents (i.e. carbon nanotubes and carbon nanofibers cost more than $1,500 per kg), provide inherently high specific surface area (theoretical value of 550 $m^2\ g^{-1}$) and are environmental friendly (Abdulridha et al., 2020). These attributes of CNCs make them an interesting prospect to use them in templating method.

1.3 Cellulose Nanocrystals

Cellulose is a type of polymer which contains β-(poly-1,4-d-glucose) monomers in their backbone chain. The chains are linked with each other by hydrogen bonding. Each cellulose microfibril contains crystalline regions segregated by amorphous domains which result from the microfibril axial defects. During the first half of 1950s, Rånby et al. (1949) demonstrated a method through which these amorphous regions can undergo acid hydrolysis or enzymatic hydrolysis. This particular process completely eliminates the amorphous domains from the cellulose microfibrills leaving out rigid, rod-like nanocrystals namely cellulose nanocrystals (CNCs) (Rånby et al., 1949). Preparation of cellulose nanocrystals from wood pulp has been demonstrated in Figure 3 (Tran et al., 2020).

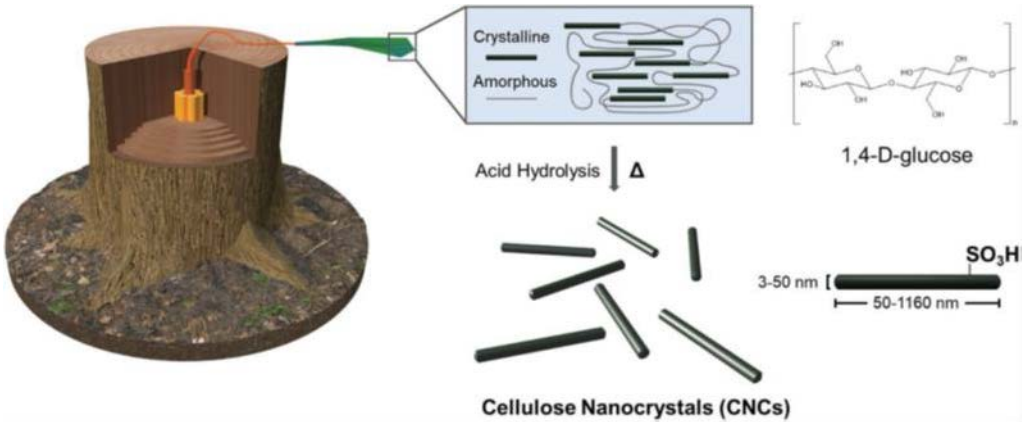

Figure 3. Steps of producing CNCs from wood pulp by eliminating amorphous region. Reproduced with the permission from Tran et al., (2020).

Different acids have been in incorporation for this specific hydrolysis treatment. However, of them sulfuric acid has been found to be more efficient in converting hydroxyl groups of the cellulose into sulfate half-ester groups locating on the surface of the CNCs. These negatively charged sulfate groups contribute towards long term colloidal stability of the CNC suspensions through electrostatic double layer repulsive force between particles. (Tran et al., 2020) By altering the synthetic strategies, the colloidal stability and interaction chemistry between particles can be controlled.

The dimensions of the cellulose nanocrystals rely mainly on the conditions applied during the acid hydrolysis treatment and the source the cellulose microfibrills are derived from. Depending on both the average length for crystalline rods has been found to be in the range of 50-1160 nm with a diameter of 3-50 nm (Tran et al., 2020). Several properties of the cellulose nanocrystals that have been extensively studied till date are their low density, improved aspect ratio, improved tensile strength along with improved axial hardness.

For its transferrable nematic structure, CNCs have been in application as effective templating agent for the past few years. There are also several other cellulose derivatives that have been used as the templating agent. Of them, hydroxypropylcellulose (HPC) and ethylcellulose (EC) have been reported to contain lyotropic chiral nematic behavior too. These two are synthesized through alkaline treatment and thereafter reaction with particular alkyl chlorides. But the ability of exhibiting chiral nematic structure at a comparatively low concentration (3-7 wt% for CNCs, 50–75 wt% for HPC, 40 wt% for EC) makes CNCs an interesting agent for templating purpose (Giese et al., 2015; Kelly et al., 2014). In addition, CNCs can also provide higher surface area, nanoscale dimensions which also make them a unique candidate for utilizing in templating.

One of the earliest attempts to use CNCs as soft templates was reported by Mann and co-workers in 2003 (Dujardin et al., 2003). The team discovered that silica/CNC composite through the addition of prehydrolyzed solution of tetramethoxysilane (TMOS) to the CNC suspensions remains birefringent with organized channel like pores even after the calcination. However, they found long range chiral nematic order missing in the calcined composite. Shin and Exarhos in 2007 made an approach for preparing porous titania through CNC templating but failed to maintain chiral order in the resultant composite (Shin and Exarhos, 2007). Alkoxysilane precursors e.g. tetramethoxysilane (TMOS) has been interestingly found to be in compatibility with the aqueous suspension of CNCs self-assembly by Shopsowitz et al., (2010). In their work they mentioned the EISA was found to take place within a narrow pH range 2.5-4. Beyond this range the silica composites become optically opaque and achiral. Shopsowitz and co-workers managed to obtain free standing, mesoporous, chiral nematic silica films through the removal of CNCs by calcination at 540º C. (Shopsowitz et al., 2010) In a similar approach, they managed to

obtain mesoporous, chiral nematic ethylene-bridged organosilica films but with different template removal technique. In this attempt, CNCs were removed by sulfuric acid treatment (6M, 100º C) (Shopsowitz et al., 2012). Organosilica films found through this approach was less brittle than the previous approach. Shopsowitz et al., (2011) also mentioned the application of chiral nematic CNC templates for producing mesoporous carbon films for a number of applications e.g. as catalysis supports and adsorption media, as electrodes in super capacitors, in energy storage device etc.

In addition to using CNCs as soft templates, recently few studies have reported the use of CNCs for hard templating or nanocasting. In a recent patent Pilyugina T. (2019) reported that combining the zeolite precursor with nanocellulose can produce mesopores in zeolite framework with high surface area. The author added two different forms of CNCs (Freeze dried and aqueous suspension) by different weight percentage to zeolite precursor with different Si to Al ratios to obtain varying outcome with higher surface area and pore volume (Pilyugina, 2019). CNC has also been successfully employed as hard templates for the fabrication of other materials e.g. chiral mesoporous silicon carbide, chiral mesoporous carbon, flexible iridescent organosilicas (Ivanova, 2015). In a more recent work, Abdulridha et al. (2020) reported the application of CNCs as hard templates in microporous Y zeolites aiming to introduce mesopores into zeolite structure. The authors found that CNCs templated Y zeolite showed enhanced resistance towards deactivation and good catalytic performance in catalytic cracking of 1,3,5-triisopropylbenzene (Abdulridha et al., 2020).

In this work, CNCs are applied as hard template in the synthesis of novel mesoporous geopolymer-based heterogeneous catalysts.

1.4 Geopolymer

The term “Geopolymer” was first described by Joseph Davidovits in 1979 (Davidovits, 1991). Geopolymers are inorganic polymers which are synthesized through “alkali activation” of aluminosilicates raw materials in a strongly alkaline solution (Davidovits, 1991). Geopolymers can be synthesized from natural clay precursors such as kaolinite or halloysite clays (Davidovits, 1991) or a number of industrial wastes such as fly ash (Buchwald et al., 2003), volcanic ash (Lemougna et al., 2011) and granulated ground blast furnace slag (GGBS) (Buchwald et al., 2003).

The geopolymerization process is described in Figure 4 (Ryu et al., 2013). The process starts with dissolution of aluminosilicate precursor into silicate and aluminate units which then polymerise into monomers forming a gel. As the concentration of these monomers increases in the reaction media, the formed monomers undergo rearrangement which results in the growing of the geopolymer framework followed by setting to a hard mass. (Duxson et al., 2007; Provis and Van Deventer, 2009)

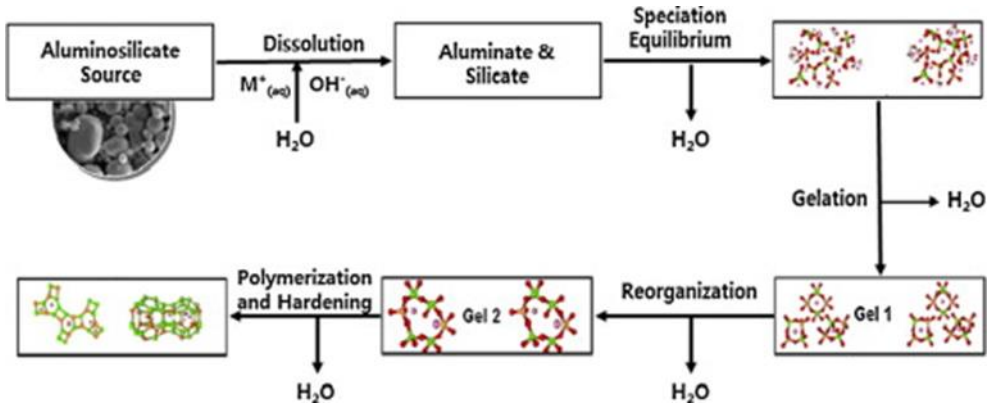

Figure 4. Geopolymerization reaction mechanism model. Reproduced with the permission from Ryu et al., (2013).

The geopolymer synthesis is usually carried out at ambient temperature (usually in the range of 40-80 °C). The resulting solid is amorphous with three dimensional structure composed of AlO_4 and SiO_4 tetrahedral units linked by their common oxygen atom (Liew et al., 2016; Sazama et al., 2011). Compensation of negative charge on the alumina tetrahedra is obtained by extra framework cation commonly Na^+ and K^+ (Alzeer and

MacKenzie, 2018; Liew et al., 2016). These cations undergo ion-exchange inducing zeolite-like properties in the geopolymers. From this perspective, geopolymers can be described as amorphous analogous of zeolite (Provis et al., 2005).

The properties of geopolymers are largely influenced by the chemical composition especially the ratio of silicate and aluminate (SiO_2/AlO_4). The typical composition for metakaolin based geopolymers has been reported as follows: $Na_2O/SiO_2 \cong 0.25$, $SiO_2/Al_2O_3 \cong 3.3$, $H_2O/Na_2O \cong 25$ (Barbosa et al., 2000). Geopolymers with the mentioned composition possess a number of interesting features most commonly their excellent mechanical properties, thermal and chemical stability which make them suitable for construction applications as environmentally friendly alternative to ordinary Portland cement (OPC) (Wu et al., 2019).

In addition, because of the ability of the geopolymer composites to be easily shaped and hardened at atmospheric temperature, specific geopolymers have got the potential to be used in particular biological operations e.g. as wear resistant joint replacement materials (Wu et al., 2019). However, it contains the risk of poisoning the surrounding biological cells because of their high alkalinity and low concentration of aluminium (Wu et al., 2019). The use of geopolymers as effective drug delivery vehicles has also been reported (Jämstorp et al., 2012). Some other applications of geopolymer as in generating antimicrobial compounds (O'Connor et al., 2010), dye carrying media (Li et al., 2006; MacKenzie and O'Leary, 2009), novel chromatography media (Alzeer and MacKenzie, 2013) have also been reported.

Recently, the use of geopolymers in heterogeneous catalysis has attracted much attention. As mentioned earlier, geopolymers are capable of undergoing ion-exchange. Through this ion-exchange process acidic, basic, redox active centres and numerous catalytically active sites can be generated in the geopolymer structure. Sometimes this can be achieved by metal substitution of Si and Al in the geopolymer framework which offer geopolymer interesting prospects for being used as heterogeneous solid catalyst. Clay-based geopolymers have been reported for their application as the support for a number of catalytically active and transition metals (Sazama et al., 2011). Sazama et al., (2011) reported the application of geopolymer as a catalyst for the selective reduction of nitrogen

oxides by ammonia and also for the total oxidation of volatile organic compounds. In their work, the team managed to generate the catalytic active sites into geopolymer framework through ion-exchange with the aqueous solutions of Fe_3^+, Co_2^+, Cu_2^+ and Pt_2^+ (Sazama et al., 2011). Gasca-Tirado et al., (2012, 2014) mentioned the addition of semiconductors (e.g. TiO_2) to the geopolymer matrix in his works for the photo-degradation of specific environmental pollutants through photochemical catalysis. In a similar attempt, Falah et al., (2016) reported the addition of a combined Cu_2O/TiO_2 into the CTAB (Cetyl trimethylammonium bromide) modified geopolymer matrix for photocatalytic oxidation of organic pollutants under UV light. Furthermore, the application of geopolymers containing Ca^{2+} as catalyst for the production of biofuels has also been reported (Sharma et al., 2015). In addition, development of clay-based geopolymers has been reported as solid acid catalysts in fine chemical applications where intrinsic acidic sites were generated within the geopolymer framework (Alzeer et al., 2017, 2016). Alzeer et al., (2016) investigated that weakly acidic silanol groups along with lower amount of Brønsted acidic sites can be generated in the geopolymer surface which provides activity and selectivity for Beckmann rearrangement of cyclohexanone oxime to caprolactam. In another study, the team reported the generation of Lewis and Brønsted acidic sites in the geopolymer structure for aromatic alkylation reactions (e.g. Friedel-Craft alkylations) (Alzeer et al., 2017).

Geopolymers provide number of benefits over other heterogeneous catalysts. Of them, one of the prime benefits are their ease of synthesis. Geopolymers can be synthesized at room temperature which make their synthesis procedure energy-efficient. In addition, they can be synthesized from naturally occurring precursors e.g. kaolin clay or industrial waste such as fly ash which also makes them environmentally benign and cost effective. Also, the acidity of the geopolymers can be controlled and different active sites can be incorporated into the geopolymer framework either by ion exchange or metal substitution of the Si and Al (Alzeer et al., 2016). But the most significant attribute is different length of pore size e.g. micro (<2 nm), meso (2-50 nm), macro (>50 nm) can be induced in their framework by changing their preliminary synthesis composition (Alzeer and MacKenzie, 2018). Thus the geopolymers provide the advantage of forming hierarchical structures by tailoring their porosity. However, this porosity cannot always be generated and controlled in a precise manner in the geopolymer matrix. In order to generate porosity of desired

size in the geopolymer framework two approach are usually followed: ‘bottom-up’ (i.e. templating methods) or ‘top-down’ (i.e. post synthetic treatments) approach (Abdulridha et al., 2020). Between the two methods, the templating methods has been found to be less energy-intensive because the post synthetic treatments require prolonged hydrothermal treatments (Abdulridha et al., 2020). Of the two existing templating method, hard templating technique has been found to contribute to the better control of the pore structure and also to the independent management of Si/Al ratio during templating method. So it can be a promising option to synthesize geopolymer of desired porous structure through hard templating technique. CNCs as a templating agent are relatively cheaper and capable of providing high specific surface area as mentioned earlier. So, using CNCs as hard template can be a fascinating option to induce mesoporosity in the geopolymer matrix which facilitates molecular transport and enhance the catalytic activity. Thus mesoporous geopolymer synthesized from CNC template would be cost effective, environmentally friendly and possess good potential as heterogeneous catalyst.

This work is focused on a novel approach of synthesizing mesoporous geopolymer with fairly high surface area through using CNCs as hard templates. Different weight percentage of CNCs were added with the geopolymer in order to obtain desired outcome. Several attempts have been made in the entire work. Few modifications were made in the geopolymer composition and also to the synthesis procedure in different attempts. Removal of the template was accomplished through the calcination of all the samples to a certain temperature and finally all the samples went through different characterization for determining structural and textural properties of the formed geopolymer-CNC composites.

2 MATERIALS AND EXPERIMENTAL METHODS

2.1 Materials and Chemicals

Chemicals used for the synthesis of geopolymer were sodium hydroxide pellets (NaOH, 99%; VWR chemicals), sodium silicate in aqueous solution (Na_2SiO_3; 35 wt% suspension in H_2O; Na_2O, 8.2%; SiO_2 27.1%; VWR chemicals), Kaolin (Sigma-Aldrich), cellulose nanocrystals (7.32wt% suspension in H_2O; BGB Ultra^{TM}), Silica fume or Silicon (IV) oxide (99%; metals basis; 325 mesh amorphous powder; Alfa Aesar), Ammonium chloride (NH_4Cl; 100%; AnalaR NORMAPUR), Ethylenediaminetetraacetic acid disodium salt dehydrate (Na_2H_2EDTA; 99.4%; AnalaR NORMAPUR)

2.2 Geopolymer Synthesis

Several attempts have been made in this whole thesis with modified composition and modified synthesis procedure in order to obtain a desired outcome. Failure to obtain a suitable result in a particular attempt led to the carrying out of the latter attempts. All the procedure with modifying chemical compositions and synthesis procedure are described in this section in a chronological order.

The molar composition of all the geopolymer samples synthesized has been represented in Table 1.

Table 1. Molar compositions of geopolymer.

Geopolymer	SiO_2/Al_2O_3	H_2O/Al_2O_3	H_2O/SiO_2	Na_2O/Al_2O_3
Geo-N	3.58	13.63	3.81	1.36
Geo-hisi	6.39	22.25	3.48	2.20

Here Geo-N is denoted for the geopolymer made with normal molar composition (e.g. SiO_2/Al_2O_3~3.5) and Geo-hisi represents the geopolymer prepared by doubling the amount of the silicon in it (SiO_2/Al_2O_3~6.5).

The geopolymer synthesis procedure and generation of their acidic form was followed from the procedure described by Alzeer et al., (2016). The procedure for the addition of CNC to the geopolymer was followed from the work of Pilyugina T. (2019) where CNC was applied as hard template with zeolite.

In the very first attempt, prior to begin the geopolymer synthesis, the measured amount of aqueous suspension of cellulose nanocrystals (CNCs) was homogenized with distilled water in a magnetic stirrer at 750 rpm for 15 minutes. After putting CNCs into stirring, the geopolymer was synthesized as follows:

Measured amount of NaOH pellets were dissolved into distilled water and the mixture was stirred continuously with a spatula until all the NaOH pellets were dissolved into the water. Then sodium silicate solution was added to the prepared NaOH solution and the overall solution was stirred for some time with the spatula which was followed by an ice bath to cool the overall solution down to room temperature. The immersion in ice bath took place for approximately 3-4 minutes. After the temperature of the solution came down to room temperature, metakaolin was then gradually added to the solution and mixed manually with the spatula at the beginning to carefully mix all the clay with the activator solution. After 7-8 minutes of manual mixing with spatula, the overall mixture became homogeneous gel like and it was then put into mechanical mixing. At the same time the homogenized CNCs suspension was gradually added to geopolymer gel. The mechanical mixer (EUROSTAR IKA®- WERKE) was used to mix the geopolymer gel with CNC for 10 minutes at 750 rpm (Note: same mixer was used in all the latter attempts). After the mixing was accomplished, the geopolymer-CNC gel was then put into plastic molds, covered with plastic bags and then was put into the oven for curing at 60º C for 24 hours. After that, the plastic molds were removed from the plastic bags and put into 40º C oven to dry for another 24 hours. The hardened geopolymer-CNC composite blocks were then removed from the molds and broken into small pieces in order to grind them in a vibratory mill and sieved to pass through a 44µm mesh to obtain fine geopolymer powder. The ground powder then underwent SEM and TEM to find out the presence of CNCs in geopolymer matrix. The weight amount (g) of the components used to synthesize geopolymer-CNC composite in this attempt is represented in Table 2.

Table 2. Chemical composition of the geopolymer-CNC sample synthesized in the 1st attempt

Sample	NaOH(g)	H_2O(g)	Na_2SiO_3(g)	Metakaolin (g)	Silica-fume (g)	CNCs (g) with H_2O (g)
Geo-N-0.8% (s)	8.25	16.0	35.0	30.0	--	10g CNCs suspension in 15g of H_2O

Here, for all the samples made in the 1st attempt or in latter attempts, 'N' represents the geopolymer synthesized with normal molar composition. 0.8wt% is the weight amount of aqueous suspension of CNCs in the geopolymer and 's' denotes for the aqueous suspension form of CNCs in this attempt and also in the latter attempts.

The 2nd attempt was made with modified composition and synthesis procedure. In this attempt, the geopolymer-CNC compounds were prepared with varied weight percentage of CNC suspension (1 wt% and 5wt% of overall compound). For 5 wt% aqueous suspensions of CNCs in the geopolymer, no water was added with the CNCs during the stirring as it was assumed that the added amount of water in the first attempt might be lowering the concentration of CNCs in the overall geopolymer-CNC mixture. The stirring was performed for 30 minutes at 750 rpm. However, stirring the CNCs without water was difficult and so the addition of water with the aqueous suspension of CNCs was again considered for the samples made with 1wt% CNC suspension. In this attempt, two samples were made with normal composition (Geo-N) and another two were made with high silicon composition (Geo-hisi). The same synthesis procedure as in the first attempt was followed for making samples with normal composition of the geopolymer but for Geo-hisi samples, silica fume powder was added at the same time of metakaolin was added to the activator solution. In this attempt also, all the prepared samples were cured in plastic molds, covered with plastic bags at 60º C for 24 hours and then removed from the plastic bag. After that all the samples were oven dried at 40º C for 48 hours because the samples did not dry properly after 24 hours period. Drying was followed by grinding

in the vibratory mill and sieving through the 44µm mesh and then all the samples were calcined in the furnace at 550º C for 1 hour with a heating rate of approx. 9º C/min to decompose and remove the CNC template in order to leave out mesopores in the geopolymer matrix. The obtained samples were then characterised by gas physisorption (N_2 adsorption-desorption) to determine the specific surface area and total pore volume. The chemical compositions tried in 2nd attempt are highlighted in Table 3.

Table 3. Chemical composition of the geopolymer-CNC samples synthesized in the 2nd attempt

Sample	NaOH(g)	H_2O(g)	Sodium silicate solution, Na_2SiO_3 (g)	Metakaolin(g)	Silica-fume(g)	CNCs (g)with H_2O (g)
Geo-N-1wt% (s)+H_2O	4.01	8.00	17.55	15.11	--	9.108g CNCs suspension in 12.1g H_2O
Geo-N-5wt% (s)	3.927	8.203	17.58	15.16	--	32.575 g CNCs suspension
Geo-hisi-1wt% (s)+H_2O	12.51	22.5	20.12	20.02	17.52	20.11 g CNCs suspension in 26 g H_2O

Geo-hisi-5wt% (s)	12.53	23.6	20.01	20.12	17.61	66.64 g suspension

Here, "+H_2O" is for the samples where the CNCs were stirred with H_2O for homogenization before adding with geopolymers.

In the 3rd attempt, four new compositions were tried. All the compositions were of geopolymers with high silicon content with different weight percentage of CNC suspension. The chemical compositions for all the samples made in the 3rd attempt are shown in Table 4.

Table 4. Chemical composition of the geopolymer-CNC composite synthesized in the 3rd attempt

Sample	NaOH(g)	H_2O(g)	Na_2SiO_3(g)	Metakaolin(g)	Silica-fume (g)	CNCs(g) with H_2O (g)
Geo-hisi-5wt% (s)	6.26	11.38	10.12	10.00	8.77	33.33g suspension
Geo-hisi-10wt% (s)	6.224	11.25	10.20	10.01	8.71	70.01g suspension
Geo-hisi-5wt%_FD	3.13	5.618	5.04	5.00	4.376	1.219g freeze dried
Geo-hisi-10wt%_FD	6.217	11.33	10.08	10.03	8.76	2.45g freeze dried

Here, 'FD' stands for freeze dried form of cellulose nanocrystals.

In this attempt (3rd), two of the samples were synthesised by adding freeze-dried CNCs (5wt% and 10wt%) with the geo-hisi and the other two by using aqueous suspension of CNCs (5wt% and 10wt%). The synthesis of the geopolymer in the 3rd attempt included the addition of NaOH pellets into the distilled water which was stirred continuously until the dissolving of all the pellets into the water. This is followed by the addition of sodium silicate solution to the prepared solution and stirring the overall solution again with the spatula for few minutes. The overall solution was then put into ice bath for 3-4 minutes. After the ice bath, the measured amount of metakaolin and fumed silica were added gradually to the mixture at the same time and the overall mixture was mixed manually with the spatula for 7-8 minutes. Then the mixture went under mechanical mixing for 15 minutes at 750 rpm. This time when the geopolymer was formed after 15 minutes of mixing, CNCs were then added to the geopolymer gel. The weighed amount CNCs (aqueous suspension and freeze-dried) was added directly to the geopolymer without pre-homogenisation. The overall mixture was then mixed for 15 minutes at 1000 rpm. After the mixing was accomplished, geopolymer-CNC gel was then put into plastic molds, covered in plastic bags and cured in 80° C for 6 hours which was followed by oven drying at 40° C for 48 hours. The hardened geopolymer blocks were then ground and sieved (125µm mesh) as described above and calcined at 550° C for 1 hour with 9° C/minute heating rate. In this particular attempt, the calcined powder was then dealuminated through acid wash following the procedure described by Alzeer et. al., (2016) in which weighed amount of calcined geopolymer-CNC composite powder was treated with 20 ml/g 0.11 M Na_2H_2EDTA for 5 hr. at 85° C. The dealuminated powder was then filtered, washed with distilled water several times and put into 40° C for overnight drying. The dried powder then went through ion-exchange with a view to catalyst preparation. The ion-exchange procedure has been described separately in latter part of this chapter. The prepared catalyst was then characterised by gas physisorption. However, the porosity values were still very low.

In the 4th attempt, a different kaolinite powder (Sigma-Aldrich) was used with several modifications in the synthesis procedure and geopolymer and CNC compositions. In addition, the weight percentage of CNCs in all those previous attempts was calculated taking the water amount in the overall mixture under consideration. In the 4th attempt, the amount of water in the overall compound was excluded during the calculation of the

weight percentage of CNCs in the geopolymer according to the work of Pilyugina T. (2019). This modification was strictly followed in the latter attempts also. Moreover, for better homogenization and avoid agglomeration of both forms of CNCs e.g. freeze dried and aqueous suspension, homogenizer (IKA®T25 digital ULTRA-TURRAX®) was used this time. In addition, composition of the geopolymer was modified in this attempt again and mixing of the geopolymer with CNCs was carried out for a much longer period in this attempt for better mixing. At the very beginning of this attempts, kaolinite clay (Sigma-Aldrich) was dehydroxylated for 12 hours at 750° C. Geopolymer was then synthesized through the dissolving of NaOH pellets into the distilled water and continuous stirring with spatula. It was followed by the addition of the sodium silicate and putting the overall solution in an ice bath for few minutes. Then dehydroxylated kaolinite powder was added to the solution for Geo-N samples and for Geo-hisi samples, fumed silica powder was also added at the same time. The overall mixture was then mixed for 7-8 minutes with the spatula and when the mixture turned into gel like it was then put into mechanical mixing at 750 rpm for 20 minutes. In the meantime, previously weighed CNCs (freeze dried and aqueous suspension) were homogenized with water through the homogenizer (IKA®T25 digital ULTRA-TURRAX®) for 15 minutes. Right after the homogenization, CNCs were mixed gradually with the geopolymer while the geopolymer was still under mechanical mixing. The overall mixture was then mixed with the mechanical mixer for another 90 minutes at 900 rpm. When the mixing was accomplished, geopolymer-CNC gel was put into plastic molds like the previous attempts, covered in plastic bags and put into 80° C oven for overnight curing. Thermally cured geopolymer blocks were then put into 60° C for drying for 48 hours. The dried, hardened blocks were then broken into small pieces and ground in the vibratory mill and passed through 44µm sieve to obtain fine geopolymer powder. The geopolymer powder then underwent TGA analysis. According to the result obtained from TGA analysis, the geopolymer powder was then calcined at 650° C for 1 hour at a heating rate of 11° C/min. The calcined powder was then ion-exchanged (described in later stage) in order to generate acidic sites in the geopolymer framework. The as prepared catalyst was characterised by N_2 physisorption for the determination of porosity values. However, this time also the porosity was found very low. Overall 10 samples were made in this particular attempt with different weight percentages of freeze dried CNCs and aqueous suspension of CNCs. All the compositions are described in Table 5.

Table 5. Chemical composition of the geopolymer-CNC composite synthesized in the 4th attempt

Sample	NaOH (g)	H_2O(g)	Na_2SiO_3(g)	Metakaolin (g)	Silica-fume (g)	CNCs (g) with H_2O (g)
Geo-N-ref	3.05	3.02	9.02	10.02	--	--
Geo-N-10wt% (s)	3.05	3.20	9.00	10.00	--	24.52g suspension in 24.0g H_2O
Geo-N-2.5wt%_FD	3.02	3.02	9.03	10.0	--	0.417g in 10g H_2O
Geo-N 5wt%_FD	3.03	3.04	9.04	10.00	--	0.8506g in 10g H_2O
Geo-N-10wt%_FD	3.05	3.04	9.00	10.01	--	1.7953 g in 16g H_2O
Geo-hisi-ref	2.49	2.98	6.52	4.99	2.51	--
Geo-hisi-10wt% (s)	2.51	3.01	6.49	5.01	2.50	19.22 g suspension in 20g H_2O

Geo-hisi-2.5wt%_FD	2.57	3.04	6.51	5.02	2.52	0.315g in 10g H_2O
Geo-hisi-5wt%_FD	2.57	3.06	6.53	5.02	2.5	0.6499 g in 10g H_2O
Geo-hisi-10wt%_FD	2.50	3.05	6.51	5.03	2.53	1.407g in 16 g of H_2O

In the 5th attempt, only 2 samples were made (geopolymer with 2.5wt % of freeze dried CNCs for both normal and high silicon molar composition). Both the chemical composition and synthesis procedure were same as the 4th attempt. In the 5th attempt, slow heating rate (2° C/minute) was used while calcining the geopolymer-CNC sample and calcination was performed with temperature ramp in this step based on the result obtained from TGA analysis of geopolymer-CNC composite in the previous attempt. All the samples prepared by this procedure were heated: from room temperature upto 150° C with a heating rate of 2° C/min and then held at that temperature for 1hour, then heated upto 250° C with the same heating rate and then held at that temperature again for 1 hour, then heated upto 450° C with the same heating rate and held at that temperature for 1 hour and finally heated upto 650° C with the same heating rate and held at that temperature for 6hours. The calcined powder then underwent N_2 adsorption-desorption analysis but unfortunately there was no significant change in the porosity values than the values obtained from the previous attempts. Table 6 represents the chemical composition of all the samples prepared in 5th attempt.

Table 6. Chemical composition of the geopolymer-CNC composite synthesized in the 5th attempt

Sample	NaOH(g)	H_2O(g)	Na_2SiO_3(g)	Metakaolin (g)	Silica-fume (g)	CNCs (g) with H_2O (g)
Geo-N-2.5wt%_FD	2.98	3.01	9.07	10.01	--	0.4136g in 10g H_2O
Geo-hisi-2.5wt%_FD	2.54	3.04	6.56	5.01	2.51	0.32g in 10g H_2O

In the 6th attempt, all the samples were prepared using 10wt% aqueous suspension of CNC with the normal molar composition of the geopolymer. Same chemical composition was followed as the 4th attempt. However, in this attempt, CNCs after the homogenization with water were sonicated for 5 minutes for all the samples. During the curing period some alterations were also made. This time the geopolymer-CNC gel after mixing was spread at the bottom surface in a plastic box as a thin layer for curing it in the oven (not in the plastic molds this time). Also while curing in the oven, the gel was sonicated for a number of times (at 1hour interval and for 5 minutes each interval) and mixed with spatula each time after sonication until all the gel got dried enough for the sonication can be carried out. The reason behind curing the geopolymer-CNC gel as thin layer and sonicating while curing was for the homogenous dispersion of the CNCs in the geopolymer matrix and also to prevent the separation of the CNCs from the geopolymer during the water evaporation which was observed while curing the samples as geopolymer blocks in the plastic molds prepared in previous attempts. In this attempt, overall 3 samples were prepared. First one was put into 85° C in the oven for curing but after 1hour the gel got sufficiently dried and then it was put into 40° C oven for further drying overnight. The 2nd sample was cured at 40° C overnight and 3rd one was cured at room temperature. The prepared geopolymer-CNC composites were then ground in a

mortar this time and calcined in the furnace for 1hour at 650° C with a heating rate of 2° C/minute. No ion-exchange was performed in this attempt. The calcined powder was characterized with different techniques afterwards. The chemical compositions of all the prepared samples is shown in Table 7.

Table 7. Chemical composition of the geopolymer-CNC composite synthesized in the 6th attempt

Sample	NaOH(g)	H_2O(g)	Na_2SiO_3(g)	Metakaolin(g)	Silica-fume(g)	CNCs(g) with H_2O(g)
Geo-N-10wt%(s)	3.03	3.00	9.04	10.00	--	24.517g suspension 25g H_2O

In this attempt the samples prepared were named after their curing temperature in the result section and so one sample was named as Geo-N-10wt%(s)-85 and the other two were named as Geo-N-10wt%(s)-40 and Geo-N-10wt%(s)-RT where 'RT' stands for room temperature.

2.3 Catalyst Preparation

The preparation procedure of the catalyst form of the geopolymer was carried out as described by Alzeer et. al., (2016). The acidic form of geopolymer was obtained through ion-exchange. Charge balancing Na^+ ions were replaced with NH_4^+ ion through ion-exchange. This is accomplished by treating 1g of geopolymer powder with 100 ml of 0.1M NH_4Cl solution at room temperature with vigorous magnetic stirring (750rpm) for 24hr. The powder was then filtered off, washed 2-3 times with freshly prepared 0.1M NH_4Cl solution and finally washed again with distilled water to get rid of any remaining ions. The powder trapped on the filter paper was then dried at 40° C overnight and the dried powder was further calcined at 550° C for 15 minutes 9° C/min in static air.

2.4 Characterization Methods

The synthesized geopolymer-CNC composites and the prepared geopolymer catalyst were characterised by a number of techniques in order to discover the structure alongside morphology of the prepared samples.

2.4.1 X-ray powder diffraction (XRD)

X-ray diffraction (XRD) is a widely used technique to find out crystal structure and also to detect impurity phases in crystalline materials. It can provide information on average grain size, strain and crystal defects (Kohli and Mittal, 2019).

For the X-ray diffraction of the powder samples, a powder Panalytical X'Pert PRO X-ray diffractometer operated at 45 kV and 40 mA was used in this work and the XRD data were analyzed by using X'pert HighScore Plus.

2.4.2 Fourier Transform Infrared Spectroscopy (FTIR)

Fourier Transform Infrared spectroscopy (FTIR) provides information about molecular fingerprint of a material. It displays a number of absorption peaks which can be used to find out the existing functional groups in a certain molecule.

In this thesis, FTIR (DRIFT) spectra were collected on powder samples in the range of 400–4000 cm^{-1} using a Bruker Vertex v80 spectrometer.

2.4.3 Raman Spectroscopy

Raman spectroscopy enables us to trace out a particular species in a component molecule based on their molecular vibrations (Welker, 2012). So, this method is capable of providing qualitative and quantitative information both and is almost analogous to the FTIR technique in terms of information obtained.

In this work, the time-gated Pico Raman spectrometer (Timegate instruments Ltd) was used to measure the Raman spectra of the geopolymers. The Pico Raman uses pulsed laser (532 nm, green) with a shot length of 150 ps. The Raman spectra were measured between

a wave number range of 100 cm^{-1} – 2100 cm^{-1} with ~5 cm^{-1} spectral resolution. The data were treated with instrument-related Matlab-based SHSGUI -software. In the background substraction AirPLS-methods were used.

2.4.4 Gas physisorption

Gas physisorption is used to obtain information on surface area of the catalyst alongside the volume of the pores and pore size distribution. The data obtained through this method are often presented in adsorption isotherm to demonstrate the amount of gas adsorbed at different partial pressure intervals at constant temperature.

In this work specific surface areas and total pore volumes were determined by N_2 physisorption at -196° C using a Micromeritics ASAP 2020 instrument. Brunauer-Emmett-Teller (BET) method was used to obtain the specific areas whereas pore size analysis was performed by Barrett-Joyner-Halenda (BJH) method. Prior conducting N_2 physisorption, all the samples were degassed under vacuum at 300° C for 2 hours.

2.4.5 Thermogravimetric - Mass Spectrometry analysis (TG-MS)

In TG-MS analysis, a TG analyzer is usually coupled with a mass spectrometer to obtain chemical and analytical details of the evolved gases or vaporization products from a sample during it's weight change at the time of thermogravimetric analysis. TG analyzer coupled with mass spectrometer can deliver information on the composition of materials, degradation and also about reaction mechanism.

In this work. TG analysis was performed using a TG analyzer (NETZSCH STA 449F3) with a heating rate 10° C/min from 28° C to 1010° C in static air (40 Ml min^{-1}). TG analyzer was coupled with the mass spectrometer (NETZSCH QMS 403) for gas analysis in order to study the thermal decomposition behavior of templated geopolymer (at a heating rate 10° C/min from 28° C to 1008° C).

2.4.6 Electron microscopy

This technique is widely used for taking the images of the solid materials. In this thesis, two different forms of electron microscopy have been used, scanning electron microscopy

(SEM) and transmission electron microscopy (TEM). In SEM, image of the surface topography of solid materials is created by the detection of reflected electrons from the material. On the other hand, in TEM, electrons that are transmitted through a thin sample are detected. In consequence, TEM can provide information about the internal structures of the material alongside the topography. TEM is able to observe details as small as individual atoms. (Inkson, 2016)

In this work, SEM was done on Pt coated samples using Zeiss Sigma FESEM and TEM was done using JEOL JEM-2200FS EFTEM/STEM. For the TEM, the sample powder was produced by grinding in ethanol using a mortar and pestle. The slurry then was dispersed on Formvar/carbon coated copper grids.

3 RESULT AND DISCUSSION

In this chapter, all the obtained results in different attempts of this thesis through various characterization techniques are presented. There are two individual sections in this chapter. In the first section, the formation of the parent geopolymer synthesized with normal molar composition is described through the detailed analysis of the geopolymer structure alongside its thermal behaviour and morphology. In the latter part, the characteristics of the formed geopolymer-CNC composites are discussed with all the obtained results. Based on the results, the characteristics of the geopolymer-CNC sample synthesized in the 6^{th} attempt with 10wt% aqueous suspension of CNCs and cured at 40° C overnight are discussed in more detail as it has been found to demonstrate some promising outcome of all the samples prepared in the whole work.

3.1 Parent Geopolymer Characterization

This section highlights the structure of the parent geopolymer synthesized with normal molar composition, its thermal behaviour and morphology based on the obtained result from XRD, FTIR analysis, Raman spectra analysis, TGA and SEM.

3.1.1 Structural analysis of the parent geopolymer by X-ray Diffraction (XRD) analysis

X-ray diffraction pattern indicates the amorphous nature of the geopolymer. The X-ray diffraction pattern of the parent geopolymer synthesized with normal molar composition is shown in Figure 5.

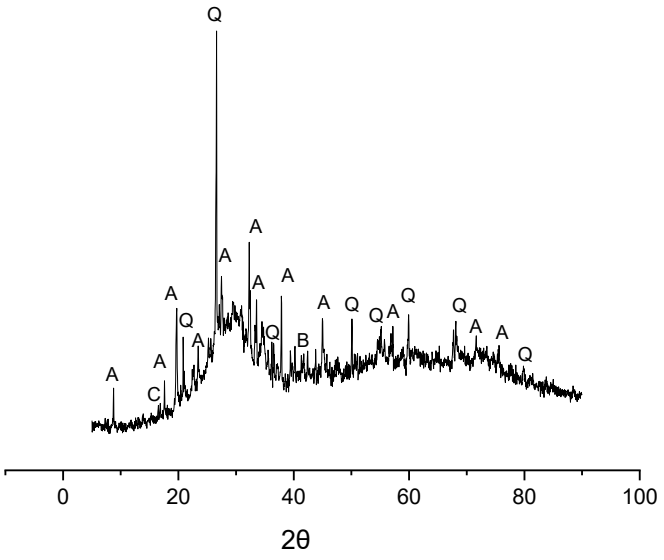

Figure 5. XRD traces of the parent geopolymer Geo-N-ref

It is evident from the Figure 5 that the parent geopolymer demonstrates an amorphous feature from 20-40° 2θ which is typical of a geopolymer. Sharp reflections indicate the presence of crystalline phases and these were identified as follows; A (potassium aluminium silicate, $KAl_3Si_3O_{11}$, ref. code: 00-046-0741), B (sodium silicate hydrate, $Na_2SiO_3.5\ H_2O$, ref. code: 00-003-0433), C (sodium carbonate, Na_2CO_3), Q (crystalline silica polymorphs quartz). Quartz are present as impurities in the geopolymer which might be included from the metakaolin clay used in synthesis. Sodium carbonate which is present as traces in the geopolymer matrix is generated from the reaction of atmospheric CO_2 with the NaOH from the geopolymer which was ensured by FTIR as described below.

3.1.2 Structural analysis of the parent geopolymer by FTIR spectra analysis

FTIR analysis indicates the formation of the geopolymers by demonstrating the presence of different inherent functional groups of geopolymer at different frequency region. FTIR transmittance spectra of the parent geopolymer sample (without CNC) is shown in Figure 6.

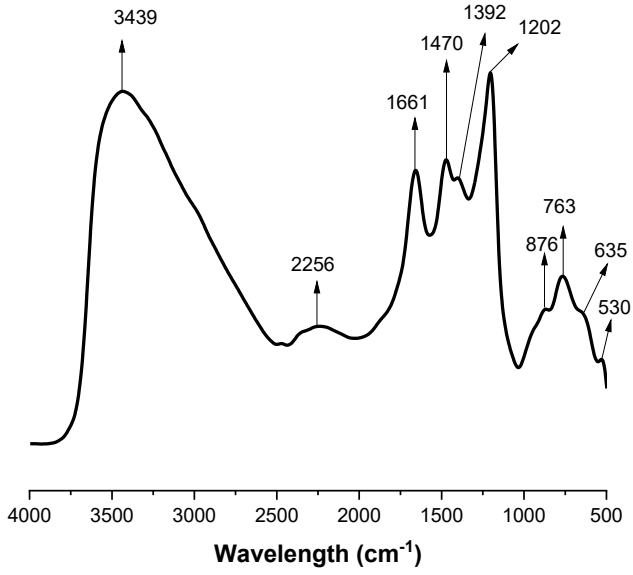

Figure 6. FTIR spectra of parent geopolymer (Geo-N-ref) synthesized with normal molar composition

The formation of the geopolymer can be ensured with the peak formed at different position with variable intensity. From the Figure 6, the strong characteristics peak around 3400-3500 cm^{-1} can arise from the –OH groups of the water present in the geopolymer and also from the other hydrogen bonded silanol nests and the small peak around 1661 cm^{-1} is attributed to the stretching vibrations of the H-OH of the adsorbed water (Alzeer et al., 2016; Król et al., 2016). The small peak around 1470 cm^{-1} indicates the formation of the carbonate by atmospheric carbonation of the geopolymer to form Na_2CO_3 (Alzeer et al., 2016; Król et al., 2016). Carbonation can also be ensured by the broad band at 2256 cm^{-1} which is ascribed to the asymmetric CO_2 stretching vibration (Alzeer et al., 2016). The peak between 1150 cm^{-1} and 1250 cm^{-1} can be associated with the stretching vibration of the Si-O-Si and Si-O-Al groups (Burduhos Nergis et al., 2020; Lee and van Deventer,

2003). The small peak between 800 cm^{-1} and 700 cm^{-1} can be ascribed to the bending vibration of tetra co-ordinated Si-O-Al bridge in the compound, while the shoulder at approximately 880cm^{-1} can be arising from the Si-OH bending mode (Alzeer et al., 2016; Chen et al., 2016). The band between 700 cm^{-1} to 600 cm^{-1} is associated to the Si-O-Si stretching, while the other band around 530 cm^{-1} can be attributed to symmetric stretching of Si−O−Al (Alzeer and MacKenzie, 2018; Burduhos Nergis et al., 2020).

3.1.3 Structural analysis of the parent geopolymer by Raman spectra analysis

The formation of the parent geopolymer was further characterised by Raman-spectroscopy. Figure 7 demonstrates the Raman spectra of the parent geopolymer sample which was collected using 100% laser power.

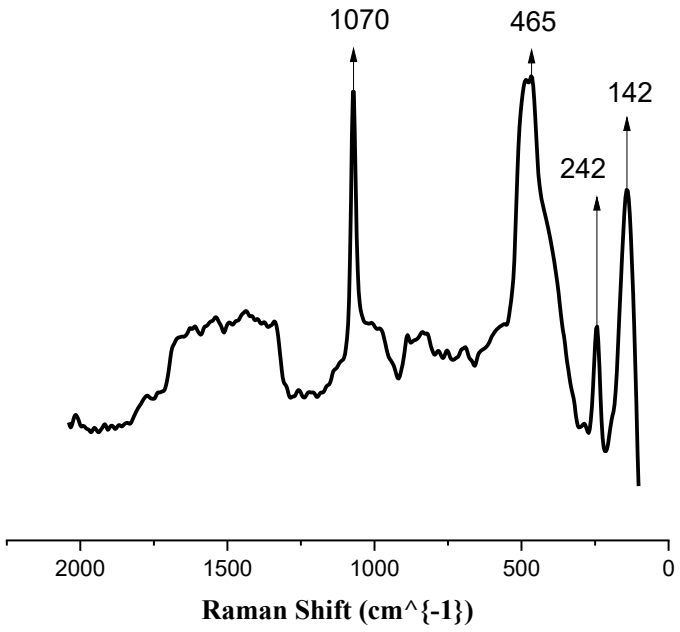

Figure 7: Raman spectra of parent geopolymer (Geo-N-ref) synthesized with normal molar composition.

Two strong characteristics bands around 465 cm^{-1} and 1070 cm^{-1} that are usually observed for typical aluminosilicate material can also be seen in the case of parent geopolymer formed (from Figure 7). The first band located around 465 cm^{-1} is broader and corresponds to the bending vibration of Si–O–Si, Si–O–Al or O–Si–O (Mierzwiński et

al., 2019). The band around 1070 cm^{-1} is comparatively narrower and ascribed to the asymmetric stretching of two silica tetrahedra connected by a bridging oxygen (T-O-T) (where T= Si or Al) (Jestel et al., 1998; Mierzwiński et al., 2019). Multiple bands designating the symmetrical stretching vibrations for Si–O–Si or Si–O–Al can also be found in the region 550–1159 cm^{-1} (Mierzwiński et al., 2019). Moreover, there are two other bands located at 242 cm^{-1} and 142 cm^{-1}. For aluminosilicate material, it was found that smaller rings give bands at higher frequencies (Yu et al., 2001). Therefore, these two bands can be ascribed to the bending mode of T-O-T (T=Si or Al) in rings that is higher than 6- or 4- membered rings; may be ascribed to the 8-membered rings or higher (Yu et al., 2001).

3.1.4 Thermal behaviour of the parent geopolymer by Thermogravimetric-Mass Spectrometry (TG-MS) analysis

Thermal behavior of the parent geopolymer sample with respect to relative weight loss as a function of temperature was determined using thermogravimetric-mass spectrometry (TG-MS) analysis under ambient condition. Figure 8 demonstrates the TG-MS graph of the parent geopolymer.

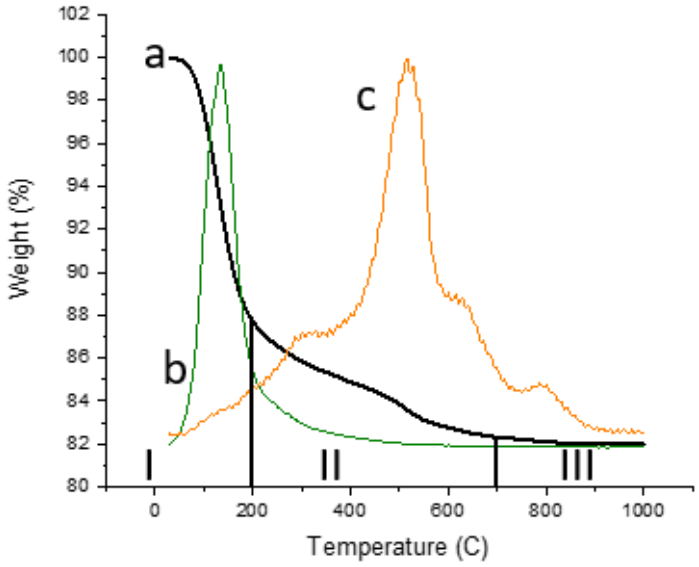

Figure 8. Representation of weight loss (%) of the (a) parent geopolymer sample (Geo-N-Ref) (black line) prepared with normal molar composition through thermogravimetric (TG) analysis and mass spectrometry (MS) graph for the mass fragment (b) m/e18 (green line) (c) m/e44 (orange line) as a function of temperature.

It is evident from the Figure (8) that there was good amount of mass loss from the parent geopolymer as a result of the thermal treatment from room temperature to 800° C. The whole temperature region (room temperature to 1000° C) of the TG-MS curve from Figure 8 is divided into three regions. The weight loss in the region I (which is below 200° C) corresponds to the evaporation of adsorbed water from the geopolymer (Lemougna et al., 2020). The peaks obtained in the mass spectrometry for mass fragment m/e18 (green line) in the temperature region below 200º C also indicates that most of the mass loss in this region was related to the elimination of water molecule from the geopolymer matrix. The rate of weight loss was comparatively rapid and most of the mass loss from the parent geopolymer took place in this region (I). There was an approximate of 12.5% mass loss occurred in the region I. In the following region (II), temperature was in the range between 200° C to 700° C. The mass loss rate slowed down in region II. Approximately 5.5% mass loss occurred in this region and this was mostly due to the degradation of sodium carbonate (Na_2CO_3) formed in the geopolymer matrix from atmospheric carbonation(Cheng-Yong et al., 2017). The peak for mass fragment m/e44 is related to the elimination of CO_2 which is supposed to be generated from the

degradation of sodium carbonate in the parent geopolymer matrix. The small peak for mass fragment m/e 44 in the temperature region 700° C - 800° C tells that little amount of degradation of sodium carbonate took place in that region also. No mass loss was observed after the temperature reached to 800° C (region III) which indicates no further presence of any thermally decomposed or volatile elements in the parent geopolymer.

3.1.5 Morphology analysis of the parent geopolymer by Scanning Electron Microscopy (SEM) technique

Figure 9 shows the microstructure of the parent geopolymer.

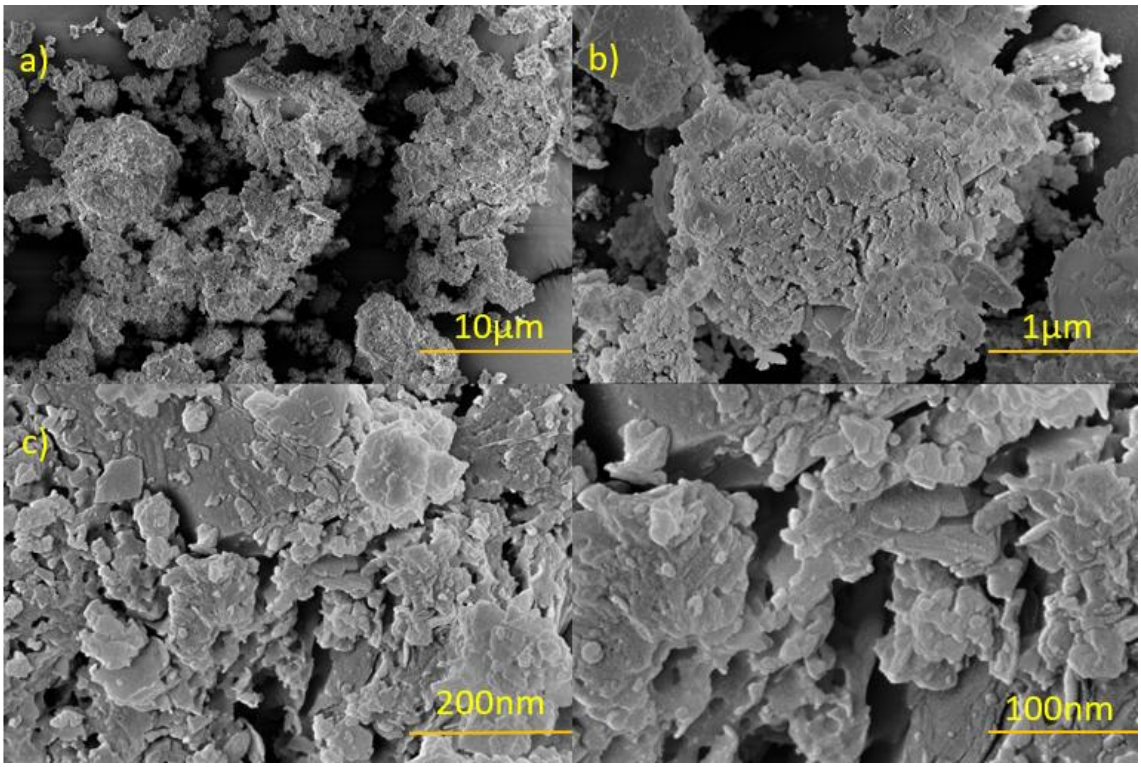

Figure 9. SEM micrographs of the parent geopolymer Geo-N-ref

The Figure 9 shows that randomly shaped round particles aggregated to form a dense structure. Some of the surface details were lost because of the freezing of the scanning to take the images. However, in the nanoscale length although some void spaces can be observed between the layers but no pores could be seen in the geopolymer matrix (Figure 9 c, d).

3.2 Characterization of Geopolymer-CNC composite

As mentioned earlier, a number of attempts have been made in this entire work to induce mesoporosity into geopolymer matrix with modified weight percentage of CNCs in the overall compounds and also with modified synthesis procedure. This section discusses textural properties e.g. pore volume and specific surface area of all the samples prepared in different attempts at the beginning. After that, the formation of geopolymer-CNC composites is discussed through the structural analysis of the samples prepared in the 6th attempt as well as their thermal behavior to indicate the degradation or decomposition of CNCs and their morphology to demonstrate the presence and distribution of CNCs in the geopolymer matrix. There were three samples in total synthesized in the 6th attempt. All of them were synthesized with normal molar composition of the geopolymer (SiO_2/Al_2O_3 ≅ 3.5) with 10wt% (weight amount in the overall geopolymer-CNCs compound) of aqueous suspension of CNCs.

3.2.1 Textural properties of the geopolymer-CNC composite measured by Gas Physisorption technique

In the 1st attempt of this thesis, no textural properties of the samples prepared were measured. The samples were characterized only by SEM and TEM. The textural properties of geopolymers-CNC composites synthesized in 2nd attempt is shown in Table 8. The samples prepared by stirring CNCs with water are named as Geo-N- 'x' wt%(s) +H_2O (x= amount of weight percentage of CNC in the geopolymer). Moreover, in the 2nd and latter attempts high silicon geopolymer samples (Geo-hisi) were prepared as this particular composition has shown to possess high porosity and acidity compared to normal composition reported by Alzeer et al., (2016, 2017).

Table 8. Textural properties of the geopolymer-CNC composites synthesized in 2nd attempt

Sample	S_{BET} (m^2/g)	V_{total} (cm^3/g)[a]	D_{pore} (nm)[b]
Geo-N-5wt%(s)	5.1775	0.025684	20.0472

Geo-N-1wt%(s)+H_2O	4.3685	0.017354	16.0649
Geo-hisi-5wt%(s)	2.2163	0.007897	18.3320
Geo-hisi-1wt% (s)+H_2O	0.7524	0.001124	--

[a] single point at $p/p_o = 0.994$

[b] measured by BJH (adsorption branch)

's' denotes the aqueous suspension form of CNC

It is observed from the Table 8 that in the 2nd attempt, the specific surface area and total pore volume of all the samples are very much lower than the desired value. Because of the low values, next attempt was made with modified chemical composition and synthesis procedure.

In the 3rd attempt, ion-exchange was performed to generate acidic sites in the geopolymer catalyst. Before ion-exchange, all the prepared samples underwent acid treatment as it was reported to introduce secondary mesopores into the geopolymer matrix (Alzeer et al., 2016). In addition, freeze dried (FD) form of CNCs was reported to induce mesoporosity with high surface area and high pore volume into zeolite materials (Pilyugina, 2019). So in the 3rd attempt, freeze dried form of CNCs were added with the geopolymer also in order achieve higher pore volume and specific surface area. However, both the pore volume and specific surface area were found low in this step also. Table 9 shows the pore volume and specific surface area of the samples synthesized in the 3rd attempt.

Table 9: Textural properties of the geopolymer-CNC composites synthesized in 3rd attempt

Sample	S_{BET} (m^2/g)	V_{total} (cm^3/g)[a]	D_{pore} (nm)[b]
Geo-hisi-5wt%(s)-IE	3.5611	0.011563	13.0303
Geo-hisi-10wt%(s)-IE	3.1547	0.011202	14.1929
Geo-hisi-10wt%-FD-IE	2.3973	0.008384	14.4085

Here IE denotes ion-exchanged geopolymer catalyst and 'FD' is for the geopolymer-CNC composites synthesized from freeze dried form of CNCs. 's' denotes the aqueous suspension form of CNC.

[a] single point at $p/p_o = 0.994$

[b] measured by BJH (adsorption branch)

In the 4th attempt, after having several modifications (as described in experimental section), no improvement was achieved on the pore volume and surface area. The textural properties of the geopolymer-CNC composite synthesized in the 4th attempt is represented in Table 10.

Table 10: Textural properties of the geopolymer-CNC composites synthesized in 4th attempt

Sample	S_{BET} (m^2/g)	V_{total} (cm^3/g)[a]	D_{pore} (nm)[b]
Geo-N-10wt%(s)-IE	1.2749	0.004062	15.8077

Geo-hisi-10wt%(s)-IE	1.1433	0.004352	15.5624
Geo-N-2.5wt%-FD-IE	1.9388	0.007097	17.7602
Geo-hisi-2.5wt%-FD-IE	1.1676	0.004235	13.7031
Geo-N-5wt%-FD-IE	1.3004	0.004903	21.4146
Geo-hisi-5wt%-FD-IE	1.0394	0.003704	14.0358
Geo-N-10wt%-FD-IE	1.5687	0.005606	14.4061
Geo-hisi-10wt%-FD-IE	1.0768	0.003351	26.0123

Here IE denotes ion-exchanged geopolymer catalyst and 'FD' is for the geopolymer-CNC composites synthesized from freeze dried form of CNCs. 's' denotes the aqueous suspension form of CNC.

[a] single point at $p/p_o = 0.995$

[b] measured by BJH (adsorption branch)

In the 5th attempt, slow heating rate (2° C/minute) was used while calcining the geopolymer-CNC composites for the removal of the CNC template according to the literature (Shopsowitz et al., 2010; Wan and Zhao, 2007). The objective was to find out whether it makes any impact to the surface area and pore volume to the geopolymer samples. Unfortunately, the porosity values remained low in the 5th attempt also which is represented in Table 11.

Table 11: Textural properties of geopolymer-CNC composites synthesized in 5th attempt

Sample	S_{BET} (m^2/g)	V_{total} (cm^3/g)[a]	D_{pore} (nm)[b]
Geo-N-2.5wt%_FD_IE	1.6082	0.002689	21.6279
Geo-hisi-2.5wt%_FD_IE	0.8547	0.001300	18.6649

Here IE denotes ion-exchanged geopolymer catalyst and 'FD' is for the geopolymer-CNC composites synthesized from freeze dried form of CNCs.

[a] single point at $p/p_o = 0.996$

[b] measured by BJH (adsorption branch)

In the 6th attempt, overall 3 samples were synthesized. All the 3 samples were prepared as flat sheets in this attempt (not as geopolymer blocks as in the previous attempts) to increase the water evaporation area to prevent the separation of CNC from the geopolymer which was observed in the samples prepared in the previous attempts. Unfortunately, in this attempt also there was no improvement in the pore volume and surface area which can be observed from Table 12.

Table 12: Textural properties of the geopolymer-CNCs composites synthesized in 6th attempt

Sample	S_{BET} (m^2/g)	V_{total} (cm^3/g)[a]	D_{pore} (nm)[b]
Geo-N-10wt%(s)-85	1.3168	0.002139	14.1631
Geo-N-10wt%(s)-40	1.3653	0.002326	21.0603

Geo-N-10wt%(s)-RT	1.3873	0.002246	23.0202

[a] single point at p/po = 0.976

[b] measured by BJH (adsorption branch)

‘s’ denotes the aqueous suspension form of CNC

All the related N_2 adsorption-desorption isotherms are attached in Appendix1.

Because of getting the low values of surface area and pore volume in all the attempts after all these modifications, samples prepared in the 6th attempt underwent further characterization through XRD, FT-IR analysis, Raman spectra analysis, SEM, TEM and TG-MS to investigate the reason behind not getting the desired outcome.

3.2.2 Structural analysis of the geopolymer-CNC composite by X-ray Diffraction (XRD) analysis

Figure 10 shows the alteration in the XRD pattern of the three geopolymer-CNC composites synthesized in the 6th attempt with respect to the parent geopolymer Geo-N-ref. Here, Geo-N-10wt%(s)-RT sample cured at room temperature, Geo-N-10wt%(s)-40 cured at 40° C overnight and the last one was cured at 85°C for 1hour and then at 40° C for overnight.

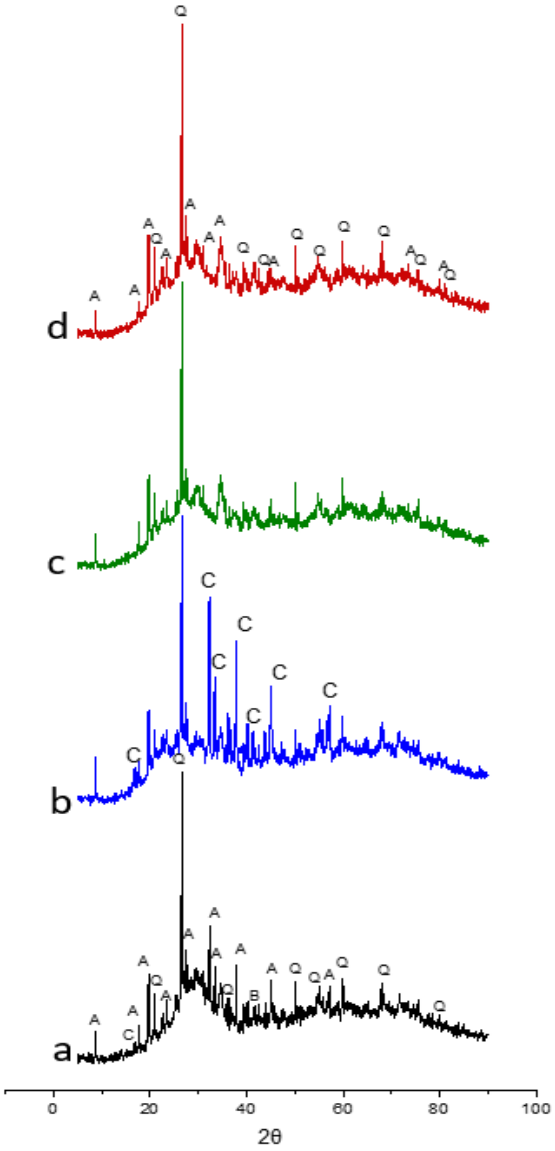

Figure 10. XRD traces of parent geopolymer sample (a) Geo-N-ref and geopolymer samples with CNCs (b) Geo-N-10wt%(s)-RT (c) Geo-N-10wt%(s)-85 (d) Geo-N-10wt%(s)-40

From the Figure 10 it can be observed that, all the geopolymers synthesized with CNCs show the same broad hump at the same 2θ position (20-40°) as the parent geopolymer which ensures the amorphous nature of the formed geopolymer-CNCs composites. The crystal elements present in all the three geopolymer matrix mainly were A (potassium aluminium silicate, $KAl_3Si_3O_{11}$, ref. code: 00-046-0741) and Q (quartz). The presence of Na_2CO_3 (C) is more obvious in the geopolymer-CNC composite that was synthesized at room temperature Geo-N-10wt%(s)-RT than in the other two composites which indicates higher degree of carbonation in this particular sample.

The prepared geopolymer-CNC composite were calcined to remove the CNC template in order to induce mesoporosity in the geopolymer matrix. The XRD pattern of calcined samples is represented in Figure 11.

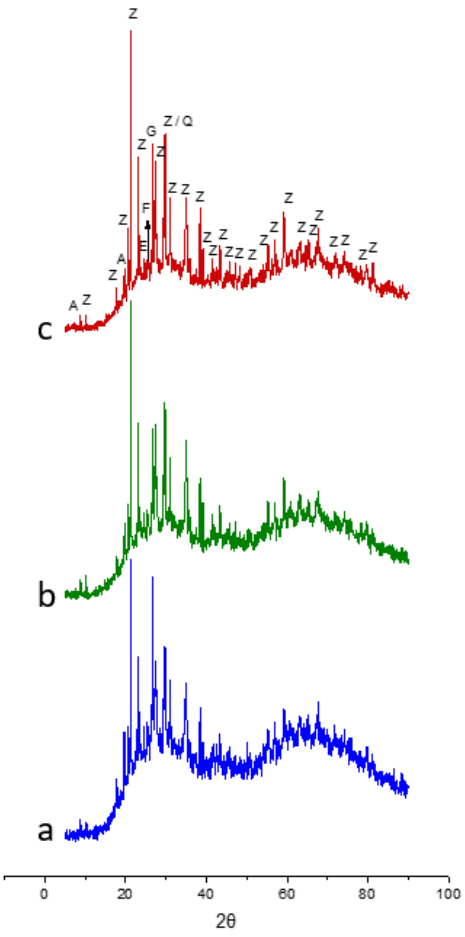

Figure 11. XRD traces of the calcined sample (a) Geo-N-10wt%(s)-RT-650C (b) Geo-N-10wt%(s)-85-650C (c) Geo-N-10wt%(s)-40-650C

All the three calcined samples show the broad background from 20-40° 2θ which ensures the existence of the amorphous feature in all three calcined samples. The three calcined samples exhibit almost the same diffraction in XRD. However, calcination caused crystallization to the geopolymer as a result some crystalline aluminosilicates (probably zeolites) were formed that are denoted by Z (crystalline sodium aluminum silicate, $Na_{7.85}$ $Al_{7.85}$ $Si_{8.15}$ O_{32}, ref. code: 01-081-8064). The peak around 27° 2θ can be ascribed to both quartz (Q) or crystalline aluminosilicates (Z) while the other peaks denoted by Z in Figure 11 are also attributed to the crystalline aluminosilicates. The presence of E (Potassium Silicon Hydride, K (Si H_3), ref. code: 04-022-7420), F (titanium dioxide, TiO_2) and traces of carbon phase (G) alongside A (Potassium Aluminum Silicate, $KAl_3Si_3O_{11}$) were also identified. Another broad hump in the 2θ position 50-80° is observed in XRD graph for all the three samples after the calcination which indicates the presence of different amorphous phase in the matrix which couldn't be identified.

3.2.3 Structural analysis of the geopolymer-CNC composite by FTIR analysis

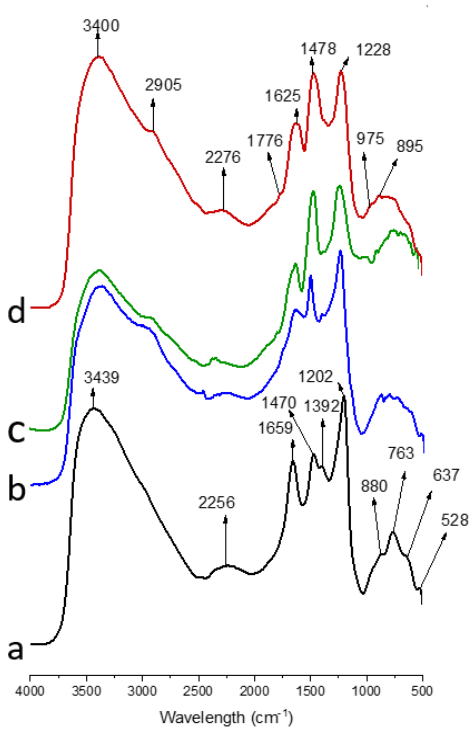

Figure 12. FTIR spectra of parent geopolymer sample (a) Geo-N-ref and geopolymer samples with CNCs (b) Geo-N-10wt%(s)-RT (c) Geo-N-10wt%(s)-85 (d) Geo-N-10wt%(s)-40

Figure 12 shows the changes in FTIR spectra between the geopolymer-CNC composites prepared in the 6th attempt and the parent geopolymer which is Geo-N-ref. From the Figure 12, the formation of geopolymer-CNC composites are ensured by the corresponding peak at different peak positions. It is evident from the Figure 12 that all the geopolymer-CNC composites show the same peaks almost at the same positions. A strong broad peak like the parent geopolymer is observed around 3400 cm^{-1} for all the geopolymer-CNC samples which is assigned to the –OH groups of the water present in the geopolymer and also to the other hydrogen bonded silanol nests along with a small peak around 1640 cm^{-1} which is due to the H-OH stretching of the adsorbed water molecule (Alzeer et al., 2016). Because of addition of CNCs with geopolymer, a new peak appears around 3450 cm^{-1} also for all the geopolymer-CNC samples that corresponds to the O-H stretching of cellulose (Chen et al., 2018). However, this peak might be overlapping here with the peak from the geopolymer alone at 3400 cm^{-1}. A small band also can be observed appearing around 2905 cm^{-1} which arises from stretching mode of C-H of the added CNCs (Fei et al., 2017). The band around 2276 cm^{-1} in the geopolymer-CNC samples correspond to the asymmetric CO_2 stretching vibration that indicates the formation of carbonate by atmospheric carbonation of the geopolymer-CNC samples like the parent geopolymer (Alzeer et al., 2016). However, the peak around 1470 cm^{-1} can be attributed to the C-H stretching of the cellulose as this peak is looking more dominant in all the geopolymer-CNC samples than in the parent geopolymer (Abdulridha et al., 2020). Cellulose shows peak around 1450 cm^{-1} and this peak from cellulose may be overlapping here with the peak around 1470cm^{-1} which is observed in the parent geopolymer that corresponds to the carbonate formed by atmospheric carbonation (Abdulridha et al., 2020; Alzeer et al., 2016). The presence of CNCs in the geopolymer matrix can be further ensured by the band around 1000 cm^{-1} (here shifted to 975cm^{-1}) which can be ascribed to C-O stretching and the other band at 1776 cm^{-1} may correspond to –OH bond in CNCs (Abdulridha et al., 2020). The small peak around 900 cm^{-1} is attributed to the rocking vibration of C-H bond in CNCs (Abdulridha et al., 2020). In addition, the strong characteristics peak at 1228 cm^{-1} that is associated with the asymmetric stretching vibration of the Si-O-Al groups further confirms the formation of the geopolymers containing cellulose nanocrystals in their matrix (Lee and van Deventer, 2003).

Figure 13 shows the FTIR spectra of the three samples that were calcined at 650° C for 1hour.

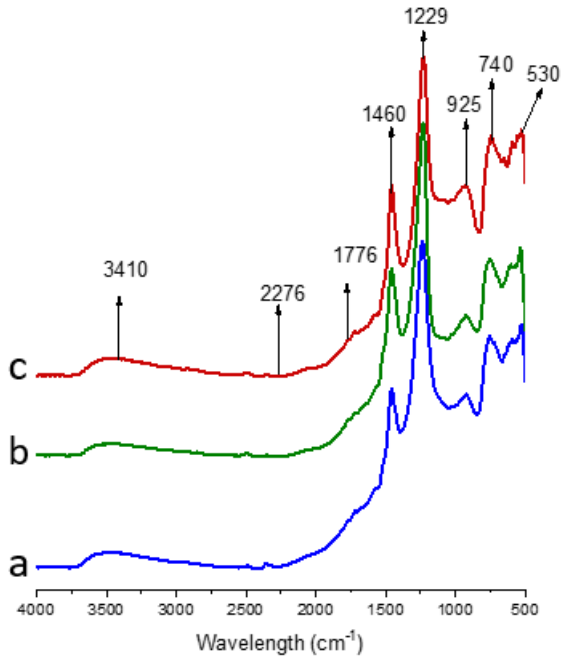

Figure 13. FTIR spectra of calcined (650°C) geopolymer samples with CNCs (a) Geo-N-10wt%(s)-RT-650C (b) Geo-N-10wt%(s)-85-650C (c) Geo-N-10wt%(s)-40-650C

The calcination of the three samples at 650° C for 1 hour resulted in the disappearance of number of peaks in the FTIR spectra of all the geopolymer-CNCs composites which is shown in Figure 13. It is evident from the Figure (13) that after the calcination, the broad peak in the 3400-3500 cm^{-1} region almost disappeared alongside the peak at 1640 cm^{-1} that shows the elimination of most of the amount of adsorbed water from the geopolymer matrix. Carbonate formation peak around 2276 cm^{-1} also disappeared after the calcination. The band located around 2905 cm^{-1}, the peak around 1470 cm^{-1}, 975 cm^{-1} and 900 cm^{-1} that corresponds to the stretching mode of C-H, C-O and rocking vibration of C-H of the CNCs got eliminated after the calcination. Although this might indicate that CNCs are eliminated from the geopolymer matrix after calcination but there is still uncertainty about the complete removal of CNCs from the geopolymer matrix as the peak at 1460 cm^{-1} and the band at 1776 cm^{-1} can still be seen from the Figure (13) which are

related to C-H stretching and –OH bond in CNCs. This shows that there might still be some CNCs remaining in the geopolymer matrix even after the calcination. However, all the geopolymer-CNCs sample show the peak around 1229 cm^{-1} and 925 cm^{-1} that are ascribed to the asymmetric stretching vibration of the Si-O-Al groups (Król et al., 2016). The bands and peaks present in 500-800 cm^{-1} region represent the other characteristic peaks of the parent geopolymer described previously.

3.2.4 Structural analysis of the geopolymer-CNC composite by raman spectra analysis

Figure 14 represents the comparison of raman bands for the three geopolymer-CNCs sample synthesized with normal molar compositions and 10wt% aqueous suspension of CNCs, cured at different temperature with respect to parent geopolymer sample. Here. raman spectra for all the samples prepared with CNCs were collected with 30% laser.

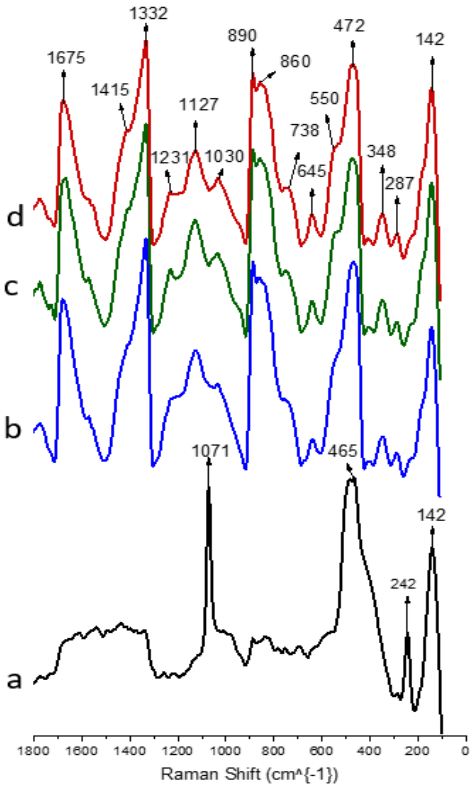

Figure 14. Raman spectra for parent geopolymer sample (a) Geo-N-Ref and geopolymer-CNC composite samples (b) Geo-N-10wt%(s)-RT (c) Geo-N-10wt%(s)-85 (d) Geo-N-10wt%(s)-40

The formation of the geopolymer-CNC composites can be further ensured by the presence of different intensity bands at various frequency regions in raman spectra. A band around 142 cm^{-1} is observed from the Figure (14) in all the three samples. Another band around 240 cm^{-1} was observed in all the samples (here shifted to 287 cm^{-1}). These two bands can be ascribed to the bending mode of T-O-T (T=Si or Al) in rings that is higher than 6- or 4- membered rings; may be ascribed to the 8-membered rings or higher likewise the parent geopolymer (Yu et al., 2001). In addition, the band around 460 cm^{-1} in the parent geopolymer is shifted slightly to 472 cm^{-1} in all the three samples which is ascribed to the bending vibration of Si–O–Si, Si–O–Al or O–Si–O of the geopolymer (Mierzwiński et al., 2019). The presence of CNCs in the geopolymer matrix can be ensured by a number of bands present in the raman spectra for all the three samples. The weak band present around 348cm^{-1} and the shoulder around 550 cm^{-1} can be correlated to some heavy atom stretching from CNCs (Agarwal et al., 2012; Wiley and Atalla, 1987). Band located around 890 cm^{-1} is attributed to the C-O-C stretching mode while the shoulder at 748 cm^{-1} could be from glucose ring deformation with the bending of glycosidic bond (Lewandowska et al., 2015; Makarem et al., 2019). The characteristic band for the parent geopolymer located at 1070 cm^{-1} overlaps with the strong cellulose band at 1127 cm^{-1} in all the geopolymer-CNCs composites. This particular band along with the shoulder around 1030 cm^{-1} represents stretching mode of C–O and C-C (Agarwal et al., 2012). Another shoulder around 1231 cm^{-1} may be ascribed to the HCC and HCO bending (Agarwal et al., 2012). Moreover, the band around 1332 cm^{-1} and the shoulder at 1415 cm^{-1} corresponding to the bending modes of CCH, OCH and COH moieties also confirm the presence of CNCs in the geopolymer matrix (Agarwal et al., 2012; E. Lewandowska et al., 2018). However, other bands around 1675 cm^{-1}, 860 cm^{-1} and 645 cm^{-1} could not be identified but they are expected to be related with the CNCs.

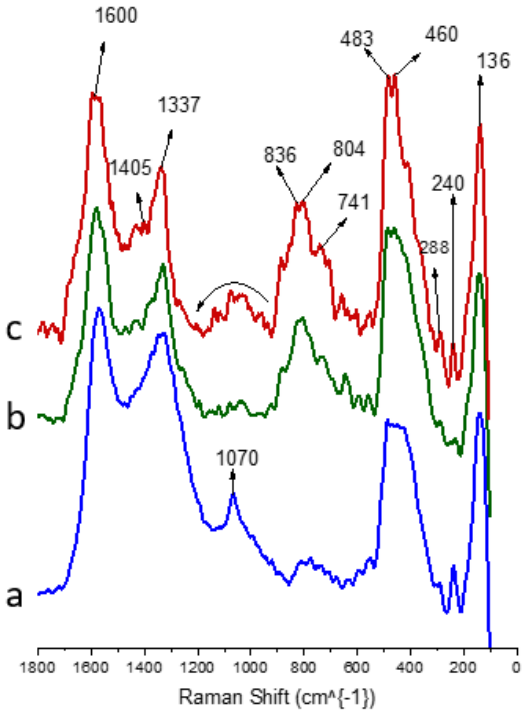

Figure 15. Raman spectra of calcined geopolymer-CNC composite samples (a) Geo-N-10wt%(s)-RT-650C (b) Geo-N-10wt%(s)-85-650C (c) Geo-N-10wt%(s)-40-650C

Figure 15 demonstrates the raman spectra of the three geopolymer-CNC samples after being calcined at 650° C for 1 hour. Like the FTIR analysis, the raman spectra of the calcined samples also shows that some bands corresponding to bending and stretching mode of different functional groups of cellulose are still present after the calcination although a number of them are seen to be disappeared. The bands located around 1332 cm^{-1} and the shoulder around 1415 cm^{-1} ascribed to the bending modes of CCH, OCH and COH are still present for all the three samples even after the calcination (Agarwal et al., 2012; E. Lewandowska et al., 2018). Although the band around 1127 cm^{-1} and its adjacent shoulders corresponding to the stretching of C-O, C-C and bending modes of HCC and HCO almost disappeared after the calcination for the samples Geo-N-10wt%s(s)-40 and Geo-N-10wt%s(s)-85 samples but a band still can be seen around 1070 cm^{-1} only for the sample cured at room temperature. This band might be generating from the CNCs or from the geopolymer that corresponds to the asymmetric stretching of T-O-T (T=Al or Si) like the parent geopolymer (Jestel et al., 1998; Mierzwiński et al., 2019). Moreover, the bands at 890 cm^{-1} and 860 cm^{-1} for the non-calcined geopolymer-CNC

composites might have shifted to 836cm^{-1} and 804 cm^{-1} for the calcined samples. The shoulder corresponding to the glucose ring deformation at 741 cm^{-1} can be also observed in the calcined samples (Makarem et al., 2019). In addition, the presence of band at 348 cm^{-1} (around 288 cm^{-1} for the calcined samples) corresponding to the heavy atom stretching from CNCs further ensures the existence of CNCs in the calcined geopolymer matrix (Agarwal et al., 2012). The other bands present at 136 cm^{-1}, 240 cm^{-1} and 460 cm^{-1} in all the calcined samples are correlated to the aluminosilicate bands (142 cm^{-1}, 242 cm^{-1} and 465 cm^{-1}) observed in the parent geopolymer described earlier. A new band is observed around 483 cm^{-1} which might be ascribed to the bending mode of Si-O-Al rings (Yu et al., 2001).

3.2.5 Thermal behaviour of the geopolymer-CNC composite by Thermogravimetric-Mass Spectrometry (TG-MS) Analysis

All the geopolymer-CNC composites underwent thermogravimetric-mass spectrometry analysis to discover the thermal behaviour of the CNCs present in the geopolymer matrix. Thermal behaviour of the geopolymer-CNC composites with respect to the parent geopolymer sample is demonstrated in Figure 16. Relative weight loss of all the samples is determined here as a function of temperature in the range room temperature to 1000° C under ambient condition.

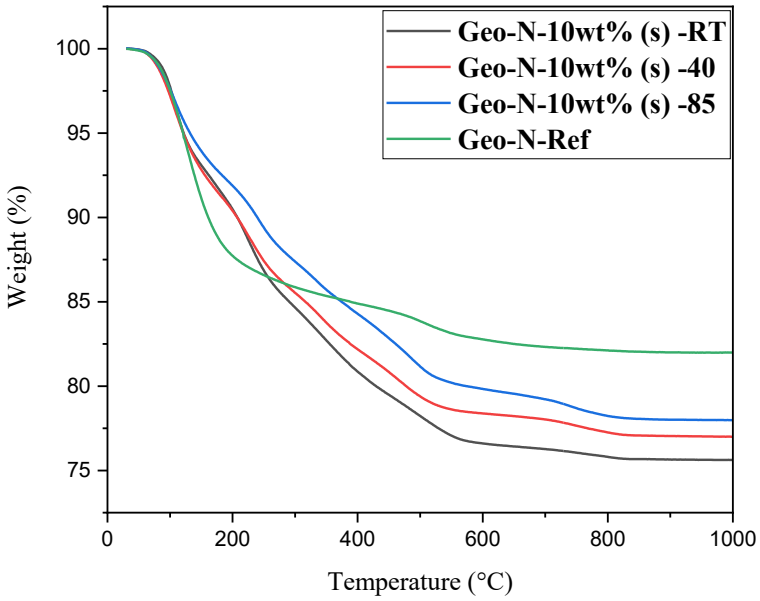

Figure 16. Comparison of weight loss (%) (as a function of temperature) of the geopolymer-CNCs composite samples: (1) Geo-N-10wt%(s)-RT (2) Geo-N-10wt%(s)-40 (3) Geo-N-10wt%(s)-85 with respect to parent geopolymer Geo-N-Ref.

From the Figure 16 it is observed that there was overall approximately 24% weight loss observed from the initial weight of all the geopolymer-CNC compounds while it was around 17% for the parent geopolymer. The weight loss (%) was higher from the geopolymer-CNC composite samples because of the presence of thermally decomposable CNCs than the parent geopolymer sample(Geo-N-Ref). Likewise the parent geopolymer sample, an approximate amount of 6% weight loss is observed initially from all the three samples between the temperature range room temperature to 200° C because of the evaporation of water from the geopolymer and also from CNCs (Lemougna et al., 2020; Trilokesh and Uppuluri, 2019). However, the decomposition of cellulose began around 200° C and significant amount of weight loss took place until the temperature reached around 650° C. This weight loss was due to the oxidation and carbonization of the free polymer CNCs alongside the degradation of carbonate material in the geopolymer matrix (Zhou et al., 2007). A lower amount of weight loss also took place from all the geopolymer-CNCs samples even after 650° C temperature which might occur from the degradation of the remaining carbonate in the geopolymer matrix. No mass loss took place after the temperature reached to 800° C.

The relative mass loss of specific element from all the geopolymer-CNC samples in different temperature region can be further ensured by their mass-spectrometry analysis. Figure 17 shows the mass spectrometry of the geopolymer-CNC composite cured at 40° C.

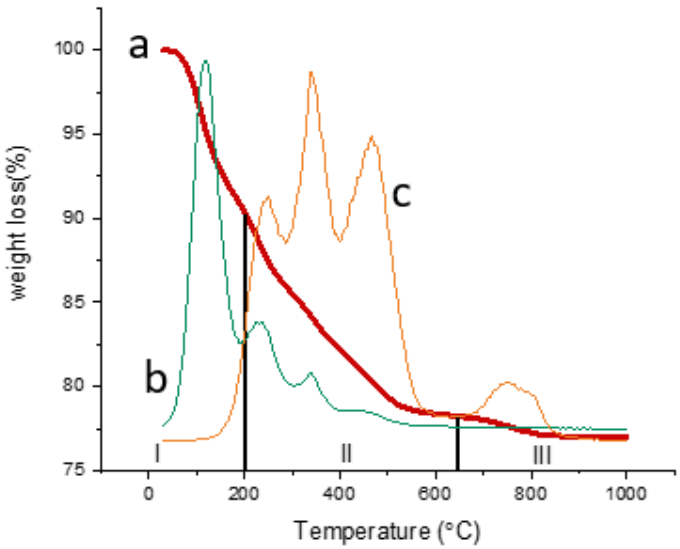

Figure 17. Representation of weight loss (%) of the (a) geopolymer-CNC composite sample Geo-N-10wt%(s)-40 (red-line) through thermogravimetric (TG) analysis and mass spectrometry (MS) graph for the mass fragment (b) m/e18 (green line) (c) m/e44 (orange line) as a function of temperature.

According to the mass spectrometry of the geopolymer-CNCs composite Geo-N-10wt% (s)-40 (Figure 17), mass loss from the geopolymer matrix in the temperature region (room temperature - 200) °C was due to the evaporation of water from geopolymer and also from CNCs (the peak for mass fragment m/e18 in this temperature region is related to water molecule). The peak for mass fragment m/e18 in the region II indicates water loss from the geopolymer-CNCs composite matrix continued until the temperature reaches to nearly 500 °C although the loss of water was much lower in amount in the region (200-700) °C. After reaching to 500°C the curve corresponding to the mass fragment m/e18 became stable which indicates no water loss took place after reaching that particular temperature. Peaks observed in the Figure (17) for mass fragment m/e44 was related to the decomposition or degradation of CO_2 element (mostly from CNCs alongside the carbonate formed due to atmospheric carbonation of geopolymer) as there were no other

particular carbon element in the geopolymer chemical composition. The peaks in the temperature region (200-700) °C for m/e 44 mass fragment indicates that the decomposition of CNCs began around 200° C and it continued to decompose until the temperature reached around 600° C. It is evident from the Figure (17) that most of the weight loss of geopolymer-CNCs samples in the temperature region (200-700) °C was due to the oxidation of CNCs from the geopolymer-CNC composite. After reaching to 600° C, the curve corresponding to the mass fragment m/e44 became stable for some time. A small peak corresponding to the mass fragment m/e44 is then observed in the mass spectra between the temperature 700° C- 800° C (Figure 17). Similar peak was observed in the mass spectrometry graph of the parent geopolymer (without CNCs) in this particular temperature region. So, this peak can be attributed to the degradation of carbonate in the geopolymer matrix.

Mass spectrometry graphs for other two samples cured at room temperature and 85° C are demonstrated in Figure 18 and Figure 19. Both the samples show similar characteristics graph like the geopolymer-CNC sample cured at 40° C. It is interesting to observe that, for the sample cured at room temperature, elimination of CO_2 element began around 100° C which was nearly 200° C for other two samples.

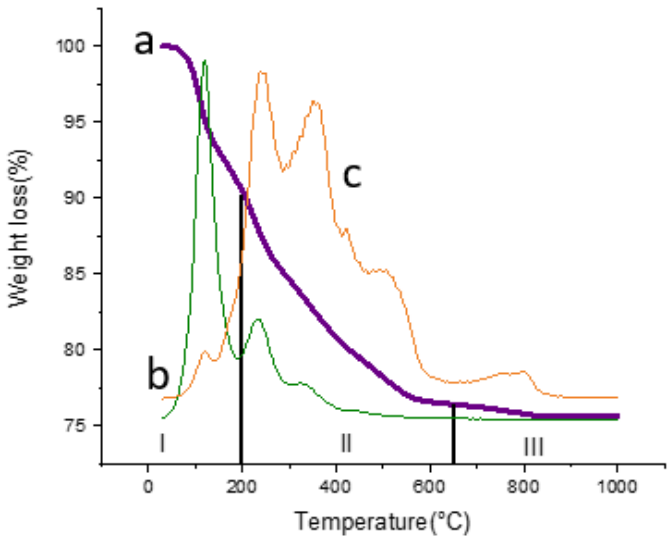

Figure 18. Representation of weight loss (%) of the (a) geopolymer-CNC composite sample Geo-N-10wt%(s)-RT (purple-line) through thermogravimetric (TG) analysis and

mass spectrometry (MS) graph for the mass fragment (b) m/e18 (green line) (c) m/e44 (orange line) as a function of temperature.

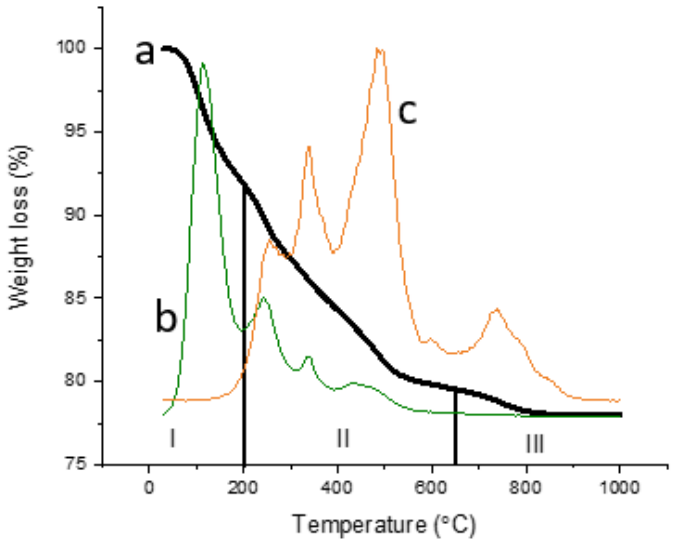

Figure 19. Representation of weight loss (%) of the (a) geopolymer-CNC composite sample Geo-N-10wt%(s)-85 (black-line) through thermogravimetric (TG) analysis and mass spectrometry (MS) graph for the mass fragment (b) m/e18 (green line) (c) m/e44 (orange line) as a function of temperature.

However, to ensure there was no decomposable mass left after being calcined to 650° C for 1 hour, all the calcined geopolymer samples underwent further TG-MS analysis. Figure 20 shows the TG-MS graph for the calcined samples.

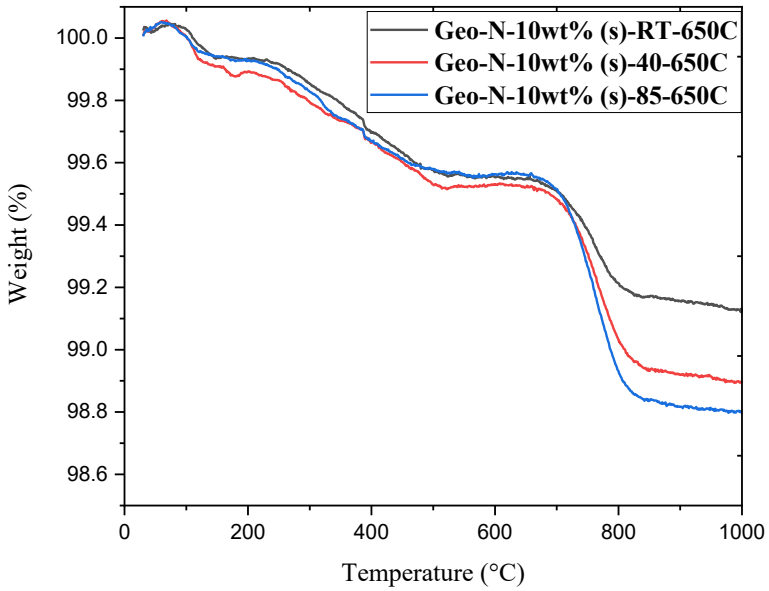

Figure 20. Comparison of weight loss (%) (as a function of temperature) of the geopolymer-CNC samples calcined at 650° C: (1) Geo-N-10wt%(s)-RT-650C (2) Geo-N-10wt%(s)-40-650C (3) Geo-N-10wt%(s)-85- 650C.

From the graph (Figure 20), it was found out that most of the decomposable mass got released from all the geopolymer samples after the calcination. However, when the temperature reached 650° C, a sudden fall in the weight loss (%) curve still is observed from the Figure (20). There was approximately (0.5- 0.8%) mass loss took place from all the 3 samples between the temperature range 650° C - 800° C. From the mass spectrometry graph shown in Figure (21) the reason behind the weight loss in this temperature region can be ensured.

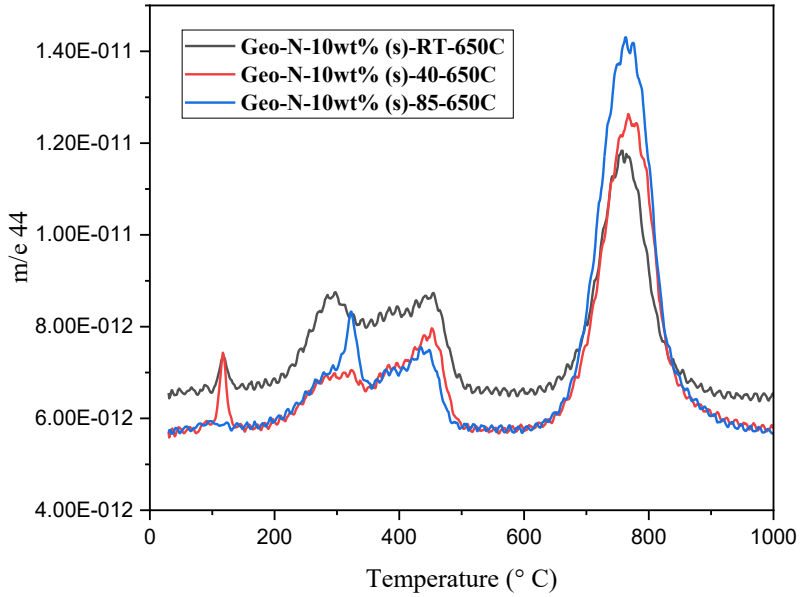

Figure 21. Mass spectrometry graph for mass fragment m/e44 as a function of temperature for all calcined geopolymer-CNCs samples: (1) Geo-N-10wt%(s)-RT-650C (2) Geo-N-10wt%(s)-40-650C (3) Geo-N-10wt%(s)-85- 650C

From the mass spectrometry analysis, it was figured out that this weight loss can be ascribed to mass fragment m/e44 which is from CO_2. From the mass spectrometry graph of the parent geopolymer, a similar spike was observed in this temperature region from which it can be assumed that, there might still be some carbonate remaining in the geopolymer matrix after the calcination which was degrading at high temperature to release CO_2 from the geopolymer.

3.2.6 Morphology analysis of the geopolymer-CNC composite by scanning electron microscopy and transmission electron microscopy

The very first geopolymer-CNC sample synthesized in the 1st attempt of this thesis was characterized only with SEM and TEM to find out the way CNC were dispersed in the geopolymer matrix. The objective was to firstly find out the presence of CNCs in the geopolymer and then to calcine the sample to remove the CNC template to obtain mesoporous geopolymer structure. However, from the geopolymer microgrpahs no CNCs were observed in the geopolymer matrix. Figure 22 shows the microstructure of the

geopolymer morphology obtained through SEM which was synthesized with 0.8% of CNCs in the very first attempt of this thesis.

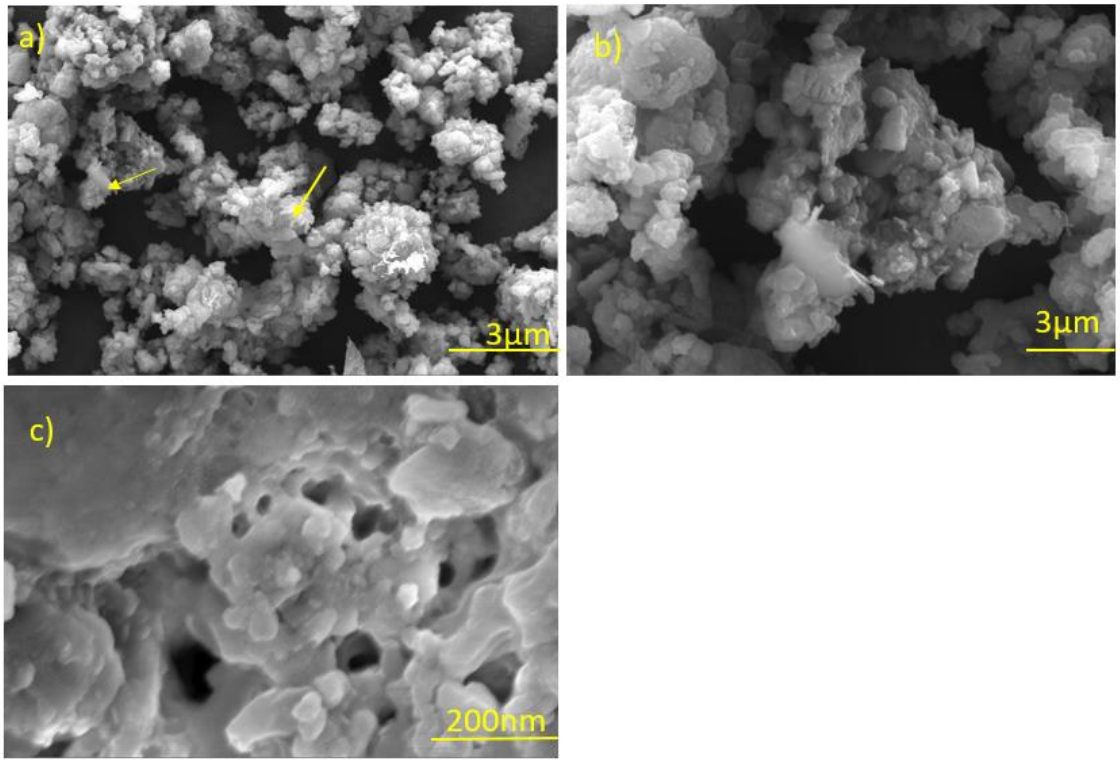

Figure 22. SEM micrographs of Geo-N-0.8wt%(s) synthesized in the 1st attempt

The formed geopolymer shows rounded particles that aggregated to form larger particles. However, from the Figure 22, no presence of CNCs was found in the geopolymer matrix. In higher magnification (Figure 22c) some voids were evident in the geopolymer matrix but these voids formed most likely during the curing process.

The prepared samples also underwent TEM analysis to find out any presence of CNCs in the geopolymer matrix. Figure 23 represents the TEM micrographs of the sample prepared in the 1st attempt in different scale length.

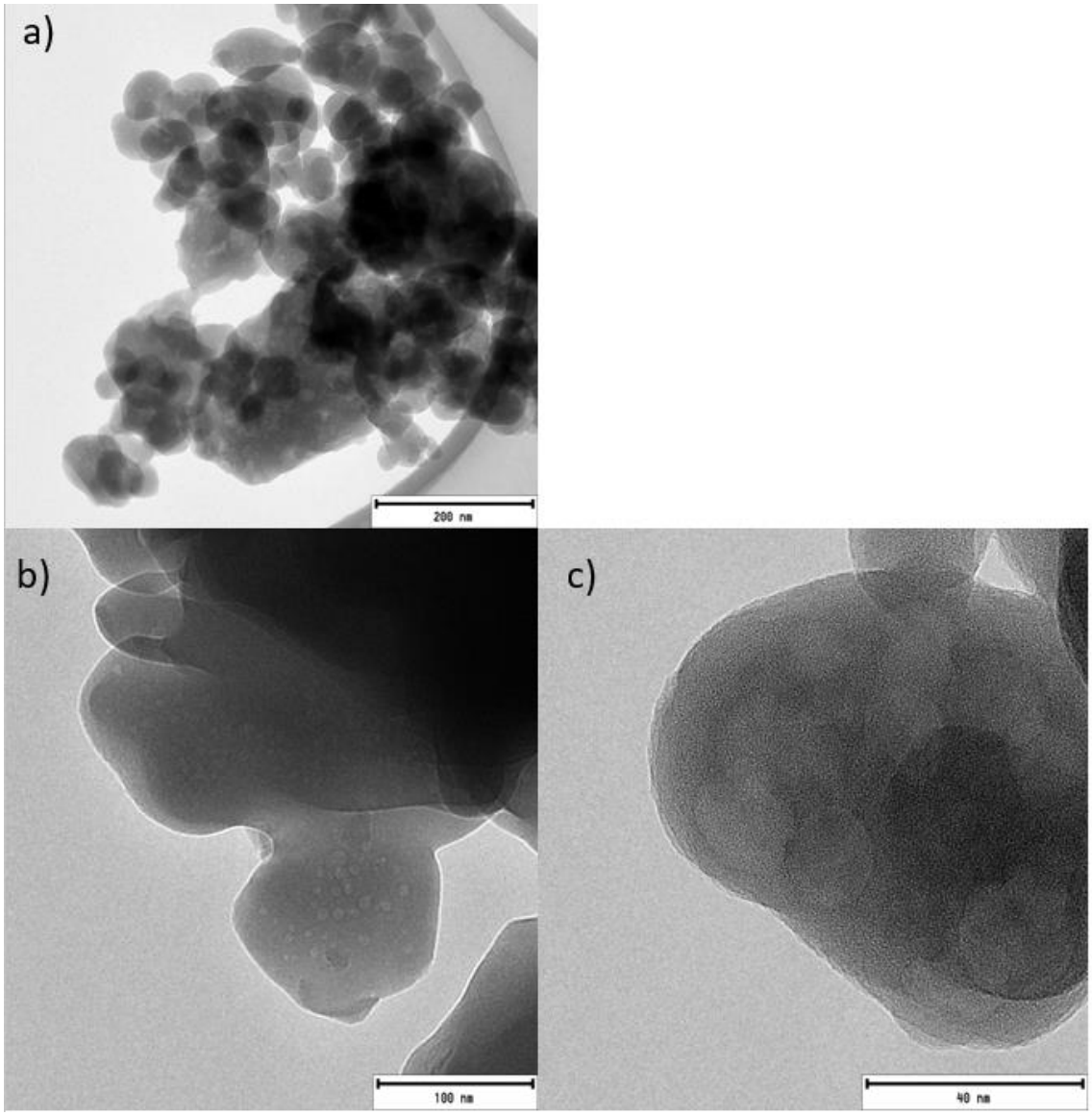

Figure 23. TEM micrographs of Geo-N-0.8wt%(s) synthesized in the 1st attempt

Figure 23 shows pores in the geopolymer matrix. But no CNCs were detected which led to make the assumption that the added amount CNCs with geopolymer might be too low and so further trials were performed with modified geopolymer-CNC composition and modified synthesis procedure.

The low porosity values of all the prepared geopolymer-CNCs sample in different attempts led to the detailed investigation of the samples prepared in the 6th attempt which is why all the three samples in the 6th attempt underwent SEM and TEM analysis to discover any underlying reason behind not getting the desired outcome. It has been found

that SEM images of the sample synthesized with 10wt% aqueous suspension of CNCs and cured in 40° C overnight in the 6th attempt produced some promising outcome unlike the other two samples. So, here the outcome of the sample Geo-N-10wt%(s)-40 will be described in a detailed manner. The SEM images of this particular sample is demonstrated in Figure 24

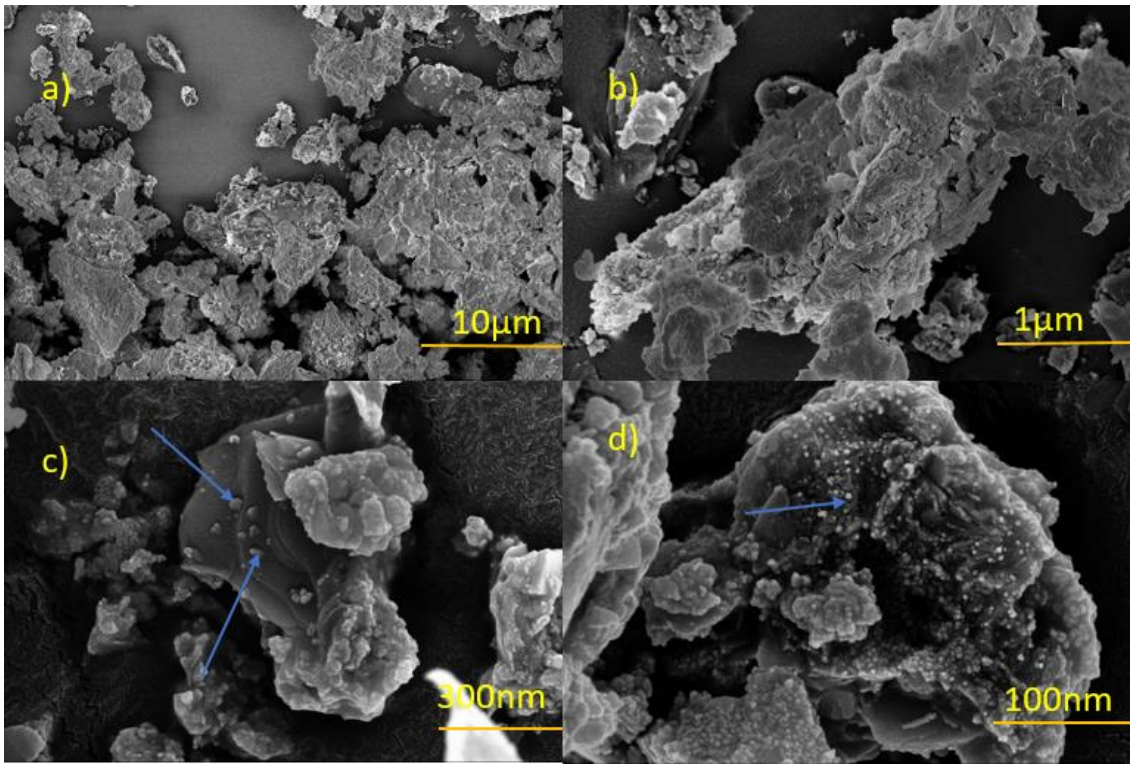

Figure 24. SEM micrographs of Geo-N-10wt%(s)-40 synthesized in the 6th attempt

Some randomly shaped aggregated particles of the geopolymer can be observed in micrometer scale length (Figure 24a, b). However, in nanometer scale (Figure 24c, d) it is observed that some round shaped (white dot) elements are present in the geopolymer matrix. These round shaped elements are expected to be the CNCs. In the Figure 24d it can be seen that, these elements are well dispersed in the geopolymer matrix.

These round particles are still observed in the geopolymer matrix even after the calcination in the SEM micrographs. Figure 25 represents the SEM micrographs of the Geo-N-10wt%(s)-40 sample which was calcined at 650° C for 1hour.

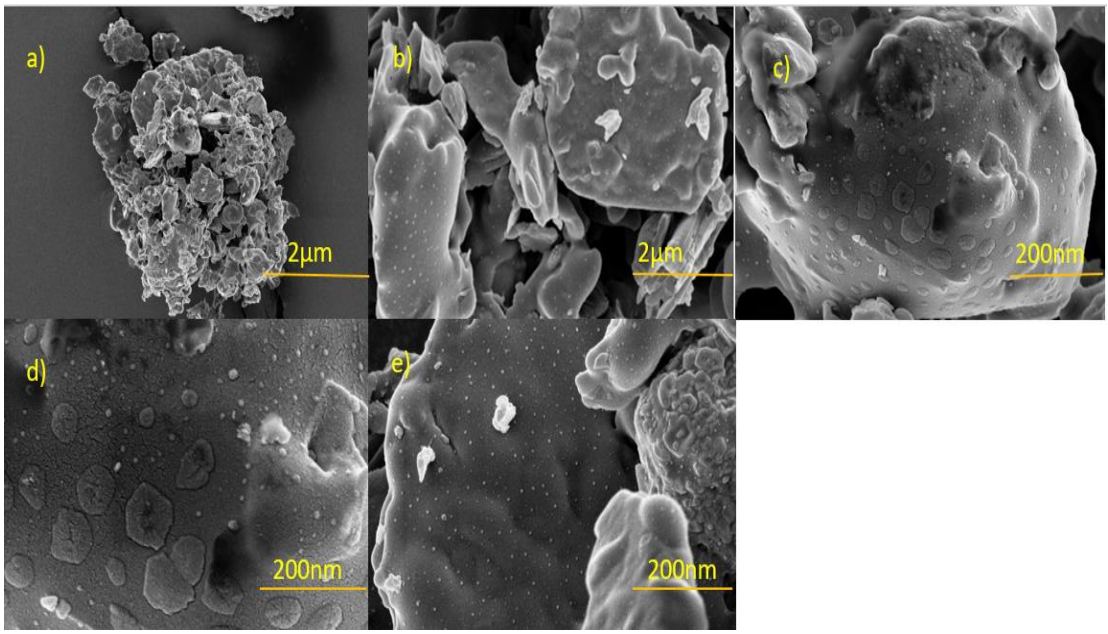

Figure 25. SEM micrograph of geopolymer-CNC composite Geo-N-10wt%(s)-40-650C which was calcined at 650° C for 1 hour (site 1)

Form the figure 25 it can be clearly seen that these round shaped particles are well dispersed all over the geopolymer particle. These particles could most probably be cellulose nanocrystals which are embedded in the geopolymer matrix. The same outcome was obtained in the SEM micrographs of the other particles of the same sample which is shown in Figure 26 which ensures that these particles are randomly but well distributed in the whole geopolymer matrix.

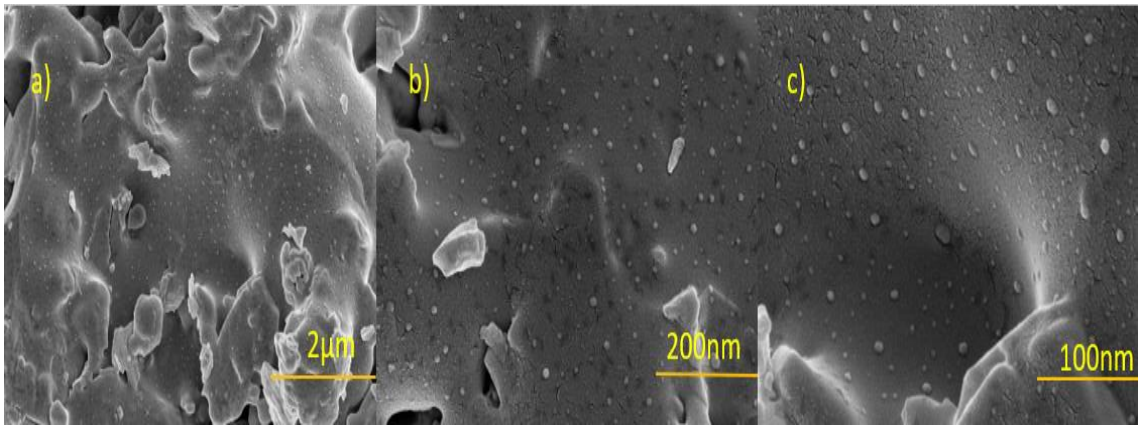

Figure 26. SEM micrograph of geopolymer-CNC composite Geo-N-10wt%(s)-40-650C which was calcined at 650° C for 1 hour (site 2)

Although Energy-Dispersive X-ray Spectroscopy (EDS) analysis could ensure the chemical nature of those round shaped elements, but all the SEM images of the mentioned sample either was obtained either at high magnification or nanoscale length and unfortunately EDS was not possible to perform accurately at this high magnification. Further analysis of these samples, perhaps using STEM would confirm the assumption that these particles are CNC and/or other formed carbonaceous phases resulted from their decomposition. Unfortunately, due to time constraints this could not be achieved in this study. Based on the assumption that these round shaped elements are CNCs, it was then assumed that the duration of the calcination in the 6th attempt to remove all the CNCs from the geopolymer matrix was not enough and for that reason CNCs were still present in the geopolymer matrix. So, Geo-N-10wt%(s)-40 sample was again calcined for at 650° C for 8hr with the same heating rate (2° C/min).

Unfortunately, this calcination for longer period did not make any changes to the surface area and porosity value again. The surface area and pore volume value for 8-hour calcined sample are given in Table 13.

Table 13: Textural properties of the of the geopolymer-CNC composite (6th attempt) which was cured at 40°C overnight and calcined (650° C) for 8 hours

Sample	S_{BET} (m^2/g)	V_{total} (cm^3/g)[a]	D_{pore} (nm)[b]
Geo-N-10wt%(s)-40-8hr	0.6468	0.000627	56.9421

[a] single point at $p/p_o = 0.977$

[b] measured by BJH (adsorption branch)

The same sample was calcined then at 650° C for 12 hours and both the 8hour and 12hour calcined samples of Geo-N-10wt%(s)-40 then underwent SEM analysis again to find out whether these round shaped elements still were existing in the geopolymer matrix after the calcination for longer period. Figure 27 and Figure 28 demonstrate the SEM micrographs of the 8hour and 12hour calcined samples.

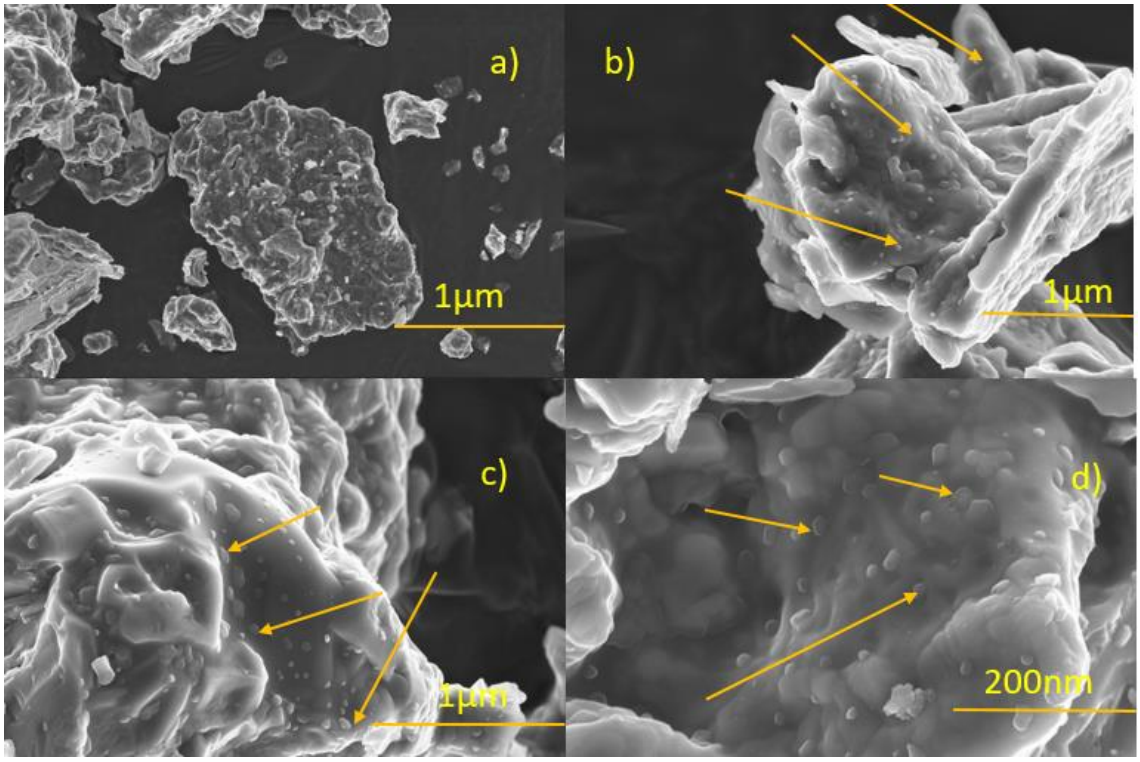

Figure 27. SEM micrograph of geopolymer-CNC composite Geo-N-10wt%(s)-40-650C(8hr) which was calcined at 650° C for 8 hour

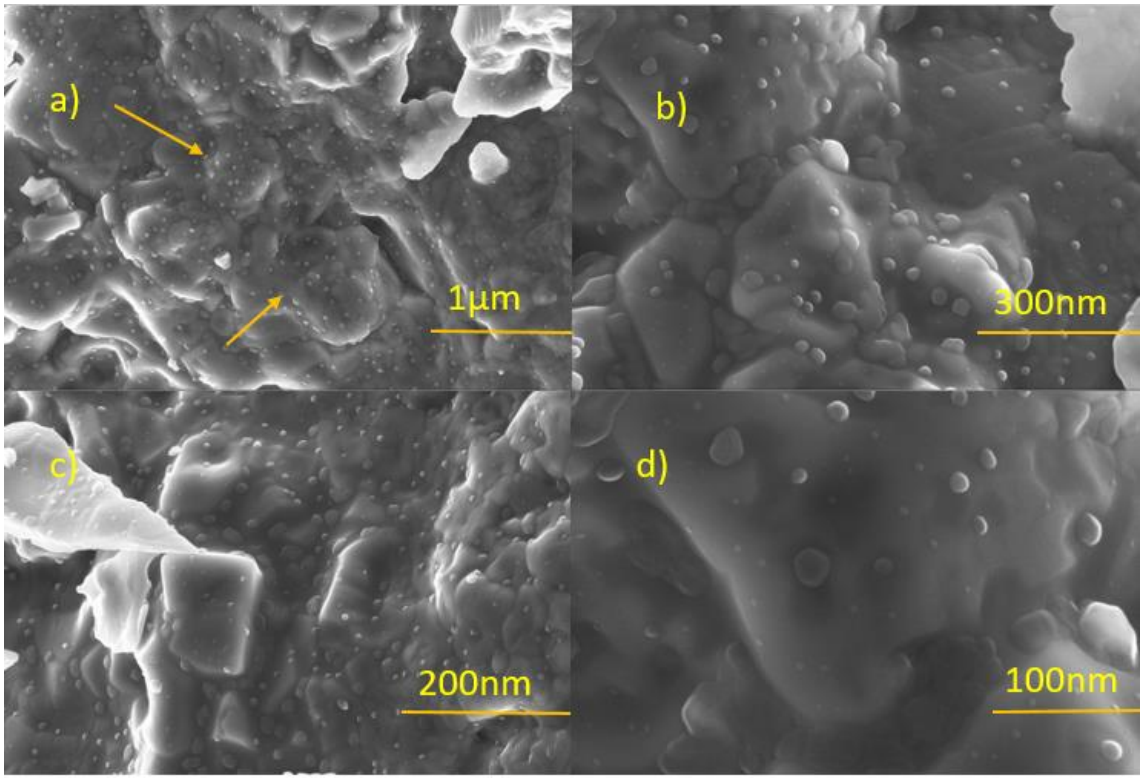

Figure 28. SEM micrograph of geopolymer-CNC composite Geo-N-10wt%(s)-40-650C(12hr) which was calcined at 650° C for 12 hour

Both the Figures (27 and 28) show that, these elements still existed in the geopolymer matrix even after the calcination for 8 and 12 hours. From both the Figure (27 and 28) it can also be observed that, because of the calcination for a longer period, some deformation took place in the geopolymer surface and some voids were created.

Based on the obtained results, few assumptions or hypotheses can be made. FTIR and Raman analysis of the prepared samples in the 6th attempt showed the peaks corresponding to CNCs even after the samples calcined for 1hour. From the SEM images also round shaped particles were observed in the geopolymer matrix of the calcined sample. Based on these outcome, the round shaped particles found in the geopolymer matrix can be assumed to be as CNCs. If these round shaped particles are the cellulose nanocrystals, then thermal decomposition was somehow not sufficient to remove the CNCs from the geopolymer which is why all the geopolymers were providing a poor pore volume and low surface area. One reason behind the CNCs not getting eliminated from the geopolymer matrix even after the thermal treatment can be the high calcination

temperature caused crystallization to the geopolymer which might resulted in a more thermally resistant phases that were providing thermal protection to the CNCs. Another assumption can be the CNCs while decomposed were transformed into some heavy hydrocarbons that were dispersed in the geopolymer matrix and not leaving the matrix.

However, if these particles are not CNCs (which is not likely) then the reason behind not finding the existence of CNCs in the geopolymer matrix is they might not be mixing well with the geopolymer even after the 90minutes of mixing. In the previous attempts of this thesis, while geopolymer-CNCs composites were being cured in the plastic moulds, a clear phase separation was observed in the geopolymer blocks. Figure 29 shows the geopolymer blocks of a sample prepared in the 4th attempt.

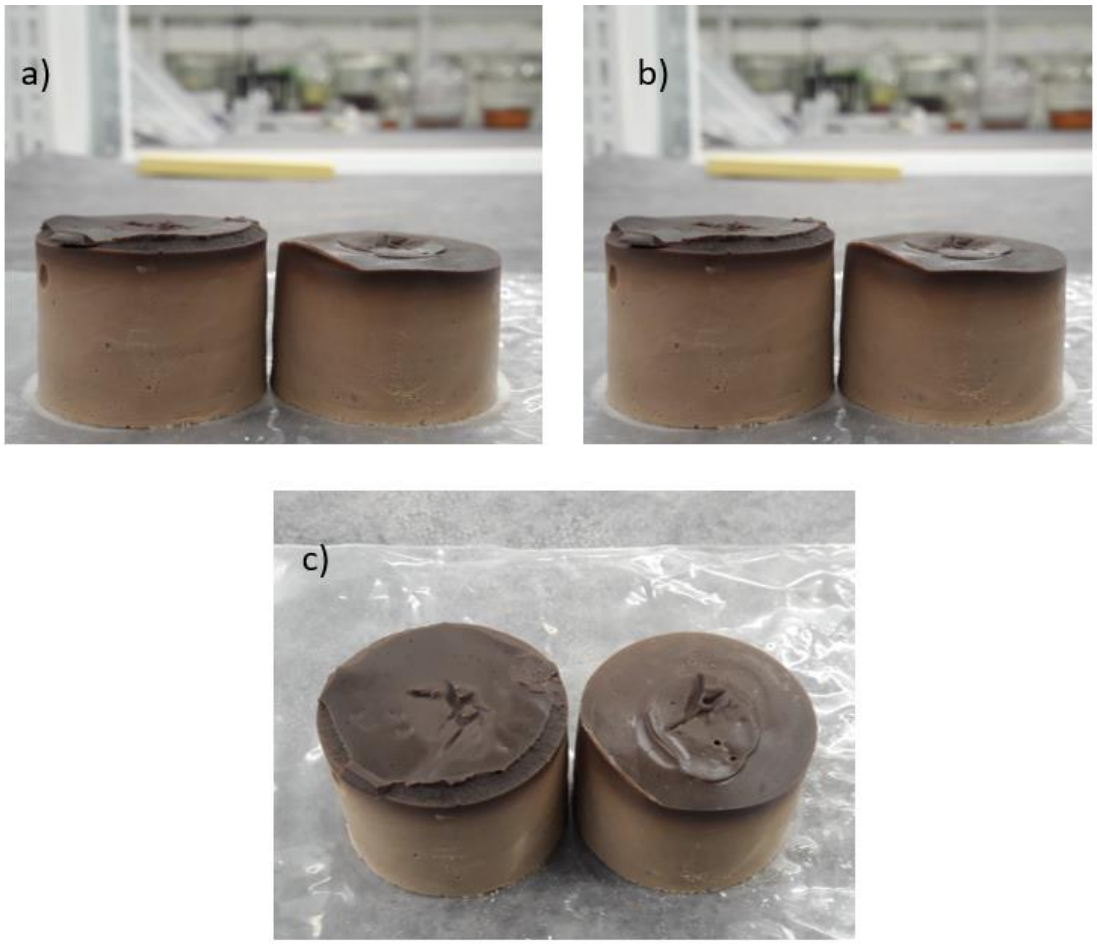

Figure 29. Blocks of geopolymer-CNC composite prepared of normal molar composition with 10wt% aqueous suspension of CNCs in the 4th attempt

The phase separation indicates that CNCs might not be homogenized well which might cause agglomeration of CNCs and thus not mixed well with the geopolymer and so while curing there were phase separation taking place during the water evaporation from the geopolymer. This phase separation might cause agglomeration of CNCs and prevent their dispersion into the geopolymer particle.

4 CONCLUSION

This work was focused on adding CNCs with geopolymer in order to achieve mesoporous geopolymer structure by using CNCs as hard templates. To our knowledge, it was a novel approach as there was no previous approach regarding using CNCs as template with geopolymer reported till date. Recently one study has reported the use of CNCs as hard templates with zeolite (Abdulridha et al., 2020).

This work included several trials where CNCs were tried to add as templates in the geopolymer matrix which would have produced significant outcome upon the removal of the template. However, despite making various modifications in each of the trial, the result was pretty dissatisfactory as the surface area and pore volume of the synthesized geopolymer-CNC composite was very poor in every trial. In the 6^{th} attempt of this thesis, an interesting outcome was obtained which showed the presence of CNCs in the geopolymer matrix in one of the three samples synthesized in that particular attempt. These CNCs were present in the geopolymer matrix even after calcining the sample at 650° C for 8hours and 12hours with a slow heating rate. If these particles are CNCs, then the following modifications can be considered for the future proceedings:

- Dissolving geopolymer-CNC composite in acidic treatment in order to decompose the CNCs through acid hydrolysis for the template removal reported by Shopsowitz et al., (2012).
- Modifying calcination technique and decompose the CNCs in a different temperature with a different heating rate.

If these particles are not CNCs, then homogenizing the CNCs for a longer period of time followed by sonication or managing a system where homogenization and sonication of the CNCs will take place at the same time during synthesis can be an effective solution to prevent agglomeration of CNCs in the geopolymer matrix. On successful templating and removal of the CNCs template, the produced mesoporous geopolymer is expected to have immense potential in various heterogeneous catalysis applications.

REFERENCES

Abdulridha, S., Jiang, J., Xu, S., Zhou, Z., Liang, H., Mao, B., Zhou, Y., Garforth, A.A., Jiao, Y., Fan, X., 2020. Cellulose nanocrystals (CNCs) as hard templates for preparing mesoporous zeolite Y assemblies with high catalytic activity. Green Chem. 22, 5115–5122. https://doi.org/10.1039/D0GC01070G

Agarwal, U., Sabo, R., Reiner, R., Clemons, C., Rudie, A., 2012. Spatially Resolved Characterization of Cellulose Nanocrystal–Polypropylene Composite by Confocal Raman Microscopy. Applied spectroscopy. https://doi.org/10.1366/11-06563

Alzeer, M., MacKenzie, K., 2013. Synthesis and mechanical properties of novel composites of inorganic polymers (geopolymers) with unidirectional natural flax fibres (phormium tenax). Applied Clay Science 75–76, 148–152. https://doi.org/10.1016/j.clay.2013.03.010

Alzeer, M.I.M., MacKenzie, K.J.D., 2018. Synthesis and Catalytic Properties of New Sustainable Aluminosilicate Heterogeneous Catalysts Derived from Fly Ash. ACS Sustainable Chem. Eng. 6, 5273–5282. https://doi.org/10.1021/acssuschemeng.7b04923

Alzeer, M.I.M., MacKenzie, K.J.D., Keyzers, R.A., 2016. Porous aluminosilicate inorganic polymers (geopolymers): a new class of environmentally benign heterogeneous solid acid catalysts. Applied Catalysis A: General 524, 173–181. https://doi.org/10.1016/j.apcata.2016.06.024

Alzeer, M.I.M., MacKenzie, K.J.D., Keyzers, R.A., 2017. Facile synthesis of new hierarchical aluminosilicate inorganic polymer solid acids and their catalytic performance in alkylation reactions. Microporous and Mesoporous Materials 241, 316–325. https://doi.org/10.1016/j.micromeso.2016.12.018

Barbosa, V.F.F., MacKenzie, K.J.D., Thaumaturgo, C., 2000. Synthesis and characterisation of materials based on inorganic polymers of alumina and silica: sodium

polysialate polymers. International Journal of Inorganic Materials 2, 309–317. https://doi.org/10.1016/S1466-6049(00)00041-6

Buchwald, A., Kaps, C., Hohmann, M., 2003. Alkali-activated binder and pozzolan cement binder-compete binder reaction or Two sides of the same story. Proceedings of the 11th International Conference on the Chemistry of Cement. https://www.researchgate.net/publication/228500946

Burduhos Nergis, D.D., Vizureanu, P., Ardelean, I., Sandu, A.V., Corbu, O.C., Matei, E., 2020. Revealing the Influence of Microparticles on Geopolymers' Synthesis and Porosity. Materials 13, 3211. https://doi.org/10.3390/ma13143211

Chen, L., Wang, Z., Wang, Y., Feng, J., 2016. Preparation and Properties of Alkali Activated Metakaolin-Based Geopolymer. Materials 9, 767. https://doi.org/10.3390/ma9090767

Chen, W., He, H., Zhu, H., Cheng, M., Li, Y., Wang, S., 2018. Thermo-Responsive Cellulose-Based Material with Switchable Wettability for Controllable Oil/Water Separation. Polymers (Basel) 10. https://doi.org/10.3390/polym10060592

Cheng-Yong, H., Yun-Ming, L., Abdullah, M.M.A.B., Hussin, K., 2017. Thermal Resistance Variations of Fly Ash Geopolymers: Foaming Responses. Scientific Reports 7, 45355. https://doi.org/10.1038/srep45355

Dai, H., Wong, E.W., Lu, Y.Z., Fan, S., Lieber, C.M., 1995. Synthesis and characterization of carbide nanorods. Nature 375, 769–772. https://doi.org/10.1038/375769a0

Davidovits, J., 1991. Geopolymers. Journal of Thermal Analysis 37, 1633–1656. https://doi.org/10.1007/BF01912193

Deutschmann, O., Knözinger, H., Kochloefl, K., Turek, T., 2011. Heterogeneous Catalysis and Solid Catalysts, 1. Fundamentals, in: Ullmann's Encyclopedia of Industrial Chemistry. American Cancer Society. https://doi.org/10.1002/14356007.a05_313.pub3

Dujardin, E., Blaseby, M., Mann, S., 2003. Synthesis of mesoporous silica by sol–gel mineralisation of cellulose nanorod nematic suspensions. J. Mater. Chem. 13, 696–699. https://doi.org/10.1039/B212689C

Dumesic, J.A., Huber, G.W., Boudart, M., 2008. Principles of Heterogeneous Catalysis, in: Handbook of Heterogeneous Catalysis. American Cancer Society. https://doi.org/10.1002/9783527610044.hetcat0001

Duxson, P., Provis, J.L., Lukey, G.C., van Deventer, J.S.J., 2007. The role of inorganic polymer technology in the development of 'green concrete.' Cement and Concrete Research 37, 1590–1597. https://doi.org/10.1016/j.cemconres.2007.08.018

Dyer, A., 2001. Zeolites, in: Buschow, K.H.J., Cahn, R.W., Flemings, M.C., Ilschner, B., Kramer, E.J., Mahajan, S., Veyssière, P. (Eds.), Encyclopedia of Materials: Science and Technology. Elsevier, Oxford, pp. 9859–9863. https://doi.org/10.1016/B0-08-043152-6/01784-8

E. Lewandowska, A., H. Inai, N., R. Ghita, O., J. Eichhorn, S., 2018. Quantitative analysis of the distribution and mixing of cellulose nanocrystals in thermoplastic composites using Raman chemical imaging. RSC Advances 8, 35831–35839. https://doi.org/10.1039/C8RA06674D

Falah, M., MacKenzie, K.J.D., Knibbe, R., Page, S.J., Hanna, J.V., 2016. New composites of nanoparticle Cu (I) oxide and titania in a novel inorganic polymer (geopolymer) matrix for destruction of dyes and hazardous organic pollutants. Journal of Hazardous Materials 318, 772–782. https://doi.org/10.1016/j.jhazmat.2016.06.016

Fei, P., Liao, L., Cheng, B., Song, J., 2017. Quantitative analysis of cellulose acetate with a high degree of substitution by FTIR and its application. Anal. Methods 9, 6194–6201. https://doi.org/10.1039/C7AY02165H

Gasca-Tirado, J.R., Manzano-Ramírez, A., Vazquez-Landaverde, P.A., Herrera-Díaz, E.I., Rodríguez-Ugarte, M.E., Rubio-Ávalos, J.C., Amigó-Borrás, V., Chávez-Páez, M.,

2014. Ion-exchanged geopolymer for photocatalytic degradation of a volatile organic compound. Materials Letters 134, 222–224. https://doi.org/10.1016/j.matlet.2014.07.090

Gasca-Tirado, R., Ramírez, A., Villaseñor-Mora, C., Muñiz-Villarreal, M.S., Zaldivar-Cadena, A.A., Rubio-Avalos, J., Amigó, V., Mendoza, R., 2012. Incorporation of photoactive TiO2 in an aluminosilicate inorganic polymer by ion exchange. Microporous and Mesoporous Materials 153, 282–287. https://doi.org/10.1016/j.micromeso.2011.11.026

Giese, M., Blusch, L.K., Khan, M.K., MacLachlan, M.J., 2015. Functional Materials from Cellulose-Derived Liquid-Crystal Templates. Angewandte Chemie International Edition 54, 2888–2910. https://doi.org/10.1002/anie.201407141

Horiuchi, Y., Toyao, T., Fujiwaki, M., Dohshi, S., Kim, T.-H., Matsuoka, M., 2015. Zeolitic imidazolate frameworks as heterogeneous catalysts for a one-pot P–C bond formation reaction via Knoevenagel condensation and phospha-Michael addition. RSC Adv. 5, 24687–24690. https://doi.org/10.1039/C5RA02410B

Humphries, A., Harris, D.H., O'connor, P., 1993. Chapter 2 The Nature of Active Sites in Zeolites: Influence on Catalyst Performance, in: Magee, J.S., Mitchell, M.M. (Eds.), Studies in Surface Science and Catalysis, Fluid Catalytic Cracking: Science and Technology. Elsevier, pp. 41–82. https://doi.org/10.1016/S0167-2991(08)63825-2

Inkson, B.J., 2016. 2 - Scanning electron microscopy (SEM) and transmission electron microscopy (TEM) for materials characterization, in: Hübschen, G., Altpeter, I., Tschuncky, R., Herrmann, H.-G. (Eds.), Materials Characterization Using Nondestructive Evaluation (NDE) Methods. Woodhead Publishing, pp. 17–43. https://doi.org/10.1016/B978-0-08-100040-3.00002-X

Ivanova, A., 2015. Nanoporous metal oxides templated by nanocrystalline cellulose (Text.PhDThesis). Ludwig-Maximilians-Universität München. https://edoc.ub.uni-muenchen.de/18642/

Jämstorp, E., Strømme, M., Bredenberg, S., 2012. Influence of drug distribution and solubility on release from geopolymer pellets--a finite element method study. J Pharm Sci 101, 1803–1810. https://doi.org/10.1002/jps.23071

Jestel, N.L., Shaver, J.M., Morris, M.D., 1998. Hyperspectral Raman Line Imaging of an Aluminosilicate Glass. Appl. Spectrosc., AS 52, 64–69. https://doi.org/10.1366%2F0003702981942339

Kelly, J.A., Giese, M., Shopsowitz, K.E., Hamad, W.Y., MacLachlan, M.J., 2014. The Development of Chiral Nematic Mesoporous Materials. Acc. Chem. Res. 47, 1088–1096. https://doi.org/10.1021/ar400243m

Kohli, R., Mittal, K.L. (Eds.), 2019. Chapter 3 - Methods for Assessing Surface Cleanliness, in: Developments in Surface Contamination and Cleaning, Volume 12. Elsevier, pp. 23–105. https://doi.org/10.1016/B978-0-12-816081-7.00003-6

Król, M., Minkiewicz, J., Mozgawa, W., 2016. IR spectroscopy studies of zeolites in geopolymeric materials derived from kaolinite. Journal of Molecular Structure, From Molecules to Molecular Materials, Biological Molecular Systems and Nanostructures 1126, 200–206. https://doi.org/10.1016/j.molstruc.2016.02.027

Lee, W.K.W., van Deventer, J.S.J., 2003. Use of Infrared Spectroscopy to Study Geopolymerization of Heterogeneous Amorphous Aluminosilicates. Langmuir 19, 8726–8734. https://doi.org/10.1021/la026127e

Lemougna, P.N., Adediran, A., Yliniemi, J., Ismailov, A., Levanen, E., Tanskanen, P., Kinnunen, P., Roning, J., Illikainen, M., 2020. Thermal stability of one-part metakaolin geopolymer composites containing high volume of spodumene tailings and glass wool. Cement and Concrete Composites 114, 103792. https://doi.org/10.1016/j.cemconcomp.2020.103792

Lemougna, P.N., MacKenzie, K.J.D., Melo, U.F.C., 2011. Synthesis and thermal properties of inorganic polymers (geopolymers) for structural and refractory applications

from volcanic ash. Ceramics International 37, 3011–3018. https://doi.org/10.1016/j.ceramint.2011.05.002

Lewandowska, A.E., Soutis, C., Savage, L., Eichhorn, S.J., 2015. Carbon fibres with ordered graphitic-like aggregate structures from a regenerated cellulose fibre precursor. Composites Science and Technology 116, 50–57. https://doi.org/10.1016/j.compscitech.2015.05.009

Li, L., Wang, S., Zhu, Z., 2006. Geopolymeric adsorbents from fly ash for dye removal from aqueous solution. Journal of Colloid and Interface Science 300, 52–59. https://doi.org/10.1016/j.jcis.2006.03.062

Li, Y., Li, L., Yu, J., 2017. Applications of Zeolites in Sustainable Chemistry. Chem 3, 928–949. https://doi.org/10.1016/j.chempr.2017.10.009

Liew, Y.-M., Heah, C.-Y., Mohd Mustafa, A.B., Kamarudin, H., 2016. Structure and properties of clay-based geopolymer cements: A review. Progress in Materials Science 83, 595–629. https://doi.org/10.1016/j.pmatsci.2016.08.002

MacKenzie, K.J.D., O'Leary, B., 2009. Inorganic polymers (geopolymers) containing acid–base indicators as possible colour-change humidity indicators. Materials Letters 63, 230–232. https://doi.org/10.1016/j.matlet.2008.09.053

Makarem, M., Lee, C.M., Kafle, K., Huang, S., Chae, I., Yang, H., Kubicki, J.D., Kim, S.H., 2019. Probing cellulose structures with vibrational spectroscopy. Cellulose 26, 35–79. https://doi.org/10.1007/s10570-018-2199-z

Marcos-Hernández, M., Villagrán, D., 2019. 11 - Mesoporous Composite Nanomaterials for Dye Removal and Other Applications, in: Kyzas, G.Z., Mitropoulos, A.C. (Eds.), Composite Nanoadsorbents, Micro and Nano Technologies. Elsevier, pp. 265–293. https://doi.org/10.1016/B978-0-12-814132-8.00012-5

Martínez, C., Corma, A., 2013. 5.05 - Zeolites, in: Reedijk, J., Poeppelmeier, K. (Eds.), Comprehensive Inorganic Chemistry II (Second Edition). Elsevier, Amsterdam, pp. 103–131. https://doi.org/10.1016/B978-0-08-097774-4.00506-4

Mierzwiński, D., Łach, M., Hebda, M., Walter, J., Szechyńska-Hebda, M., Mikuła, J., 2019. Thermal phenomena of alkali-activated metakaolin studied with a negative temperature coefficient system. J Therm Anal Calorim 138, 4167–4175. https://doi.org/10.1007/s10973-019-08471-7

O'Connor, S.J., MacKenzie, K.J.D., Smith, M.E., Hanna, J.V., 2010. Ion exchange in the charge-balancing sites of aluminosilicate inorganic polymers. J. Mater. Chem. 20, 10234–10240. https://doi.org/10.1039/C0JM01254H

Pilyugina, T., 2019. Mesoporous zeolites and methods for the synthesis thereof - Patent US-10272418-B2 - PubChem [WWW Document], n.d. URL https://pubchem.ncbi.nlm.nih.gov/patent/US-10272418-B2 (accessed 12.8.20).

Pinkert, A., Marsh, K.N., Pang, S., Staiger, M.P., 2009. Ionic Liquids and Their Interaction with Cellulose. Chem. Rev. 109, 6712–6728. https://doi.org/10.1021/cr9001947

Provis, J.L., Lukey, G.C., van Deventer, J.S.J., 2005. Do Geopolymers Actually Contain Nanocrystalline Zeolites? A Reexamination of Existing Results. Chem. Mater. 17, 3075–3085. https://doi.org/10.1021/cm050230i

Provis, J.L., Van Deventer, J.S.J., 2009. 1 - Introduction to geopolymers, in: Provis, John L., van Deventer, J.S.J. (Eds.), Geopolymers, Woodhead Publishing Series in Civil and Structural Engineering. Woodhead Publishing, pp. 1–11. https://doi.org/10.1533/9781845696382.1

Rånby, B.G., Banderet, A., Sillén, L.G., 1949. Aqueous Colloidal Solutions of Cellulose Micelles. Acta Chem. Scand. 3, 649–650. https://doi.org/10.3891/acta.chem.scand.03-0649

Ryu, G.S., Lee, Y.B., Koh, K.T., Chung, Y.S., 2013. The mechanical properties of fly ash-based geopolymer concrete with alkaline activators. Construction and Building Materials 47, 409–418. https://doi.org/10.1016/j.conbuildmat.2013.05.069

Sazama, P., Bortnovsky, O., Dědeček, J., Tvarůžková, Z., Sobalík, Z., 2011. Geopolymer based catalysts—New group of catalytic materials. Catalysis Today, Innovations driven by catalysis - Selected papers from TOCAT6 / APCAT5 164, 92–99. https://doi.org/10.1016/j.cattod.2010.09.008

Sharma, S., Medpelli, D., Chen, S., Seo, D.-K., 2015. Calcium-modified hierarchically porous aluminosilicate geopolymer as a highly efficient regenerable catalyst for biodiesel production. RSC Adv. 5, 65454–65461. https://doi.org/10.1039/C5RA01823D

Shin, Y., Exarhos, G.J., 2007. Template synthesis of porous titania using cellulose nanocrystals. Materials Letters 61, pp. 2594–2597. https://doi.org/10.1016/j.matlet.2006.10.005

Shopsowitz, K.E., Hamad, W.Y., MacLachlan, M.J., 2011. Chiral Nematic Mesoporous Carbon Derived From Nanocrystalline Cellulose. Angewandte Chemie International Edition 50, pp. 10991–10995. https://doi.org/10.1002/anie.201105479

Shopsowitz, K.E., Hamad, W.Y., MacLachlan, M.J., 2012. Flexible and Iridescent Chiral Nematic Mesoporous Organosilica Films. J. Am. Chem. Soc. 134, pp. 867–870. https://doi.org/10.1021/ja210355v

Shopsowitz, K.E., Qi, H., Hamad, W.Y., Maclachlan, M.J., 2010. Free-standing mesoporous silica films with tunable chiral nematic structures. Nature 468, pp. 422–425. https://doi.org/10.1038/nature09540

Sing, K.S.W., 1991. Characterization Of Porous Solids: An Introductory Survey, in: Rodriguez-Reinoso, F., Rouquerol, J., Sing, K. S. W., Unger, K.K. (Eds.), Studies in Surface Science and Catalysis, Characterization of Porous Solids II. Elsevier, pp. 1–9. https://doi.org/10.1016/S0167-2991(08)61303-8

Tran, A., Boott, C.E., MacLachlan, M.J., 2020. Understanding the Self-Assembly of Cellulose Nanocrystals—Toward Chiral Photonic Materials. Adv. Mater. 1905876. https://doi.org/10.1002/adma.201905876

Trilokesh, C., Uppuluri, K.B., 2019. Isolation and characterization of cellulose nanocrystals from jackfruit peel. Scientific Reports 9, 16709. https://doi.org/10.1038/s41598-019-53412-x

Wan, Y., Zhao, D., 2007. On the controllable soft-templating approach to mesoporous silicates. Chem. Rev. 107, pp. 2821–2860. https://doi.org/10.1021/cr068020s

Weckhuysen, B.M., Yu, J., 2015. Recent advances in zeolite chemistry and catalysis. Chem. Soc. Rev. 44, pp. 7022–7024. https://doi.org/10.1039/C5CS90100F

Welker, R.W., 2012. Chapter 4 - Size Analysis and Identification of Particles, in: Kohli, R., Mittal, K.L. (Eds.), Developments in Surface Contamination and Cleaning. William Andrew Publishing, Oxford, pp. 179–213. https://doi.org/10.1016/B978-1-4377-7883-0.00004-3

Wiley, J.H., Atalla, R.H., 1987. Raman Spectra of Celluloses, in: The Structures of Cellulose, ACS Symposium Series. American Chemical Society, pp. 151–168. https://doi.org/10.1021/bk-1987-0340.ch008

Wu, Y., Lu, B., Bai, T., Wang, H., Du, F., Zhang, Y., Cai, L., Jiang, C., Wang, W., 2019. Geopolymer, green alkali activated cementitious material: Synthesis, applications and challenges. Construction and Building Materials 224, pp. 930–949. https://doi.org/10.1016/j.conbuildmat.2019.07.112

Xie, Y., Kocaefe, D., Chen, C., Kocaefe, Y., 2016. Review of Research on Template Methods in Preparation of Nanomaterials [WWW Document]. Journal of Nanomaterials. https://doi.org/10.1155/2016/2302595

Yang, Z., Zhang, Y., Schnepp, Z., 2015. Soft and hard templating of graphitic carbon nitride. J. Mater. Chem. A 3, pp. 14081–14092. https://doi.org/10.1039/C5TA02156A

Yu, Y., Xiong, G., Li, C., Xiao, F.-S., 2001. Characterization of aluminosilicate zeolites by UV Raman spectroscopy. Microporous and Mesoporous Materials 46, pp. 23–34. https://doi.org/10.1016/S1387-1811(01)00271-2

Zhou, Y., Ding, E.-Y., Li, W.-D., 2007. Synthesis of TiO2 nanocubes induced by cellulose nanocrystal (CNC) at low temperature. Materials Letters 61, pp. 5050–5052. https://doi.org/10.1016/j.matlet.2007.04.001

Zhu, K., Sun, J., Zhang, H., Liu, J., Wang, Y., 2012. Carbon as a hard template for nano material catalysts. Journal of Natural Gas Chemistry 21, pp. 215–232. https://doi.org/10.1016/S1003-9953(11)60357-5

Zhu, L., Liu, X.-Q., Jiang, H.-L., Sun, L.-B., 2017. Metal–Organic Frameworks for Heterogeneous Basic Catalysis. Chem. Rev. 117, pp. 8129–8176. https://doi.org/10.1021/acs.chemrev.7b00091

Appendix 1. N_2 adsorption-desorption isotherms of all the samples synthesized in different attempts

2nd attempt:

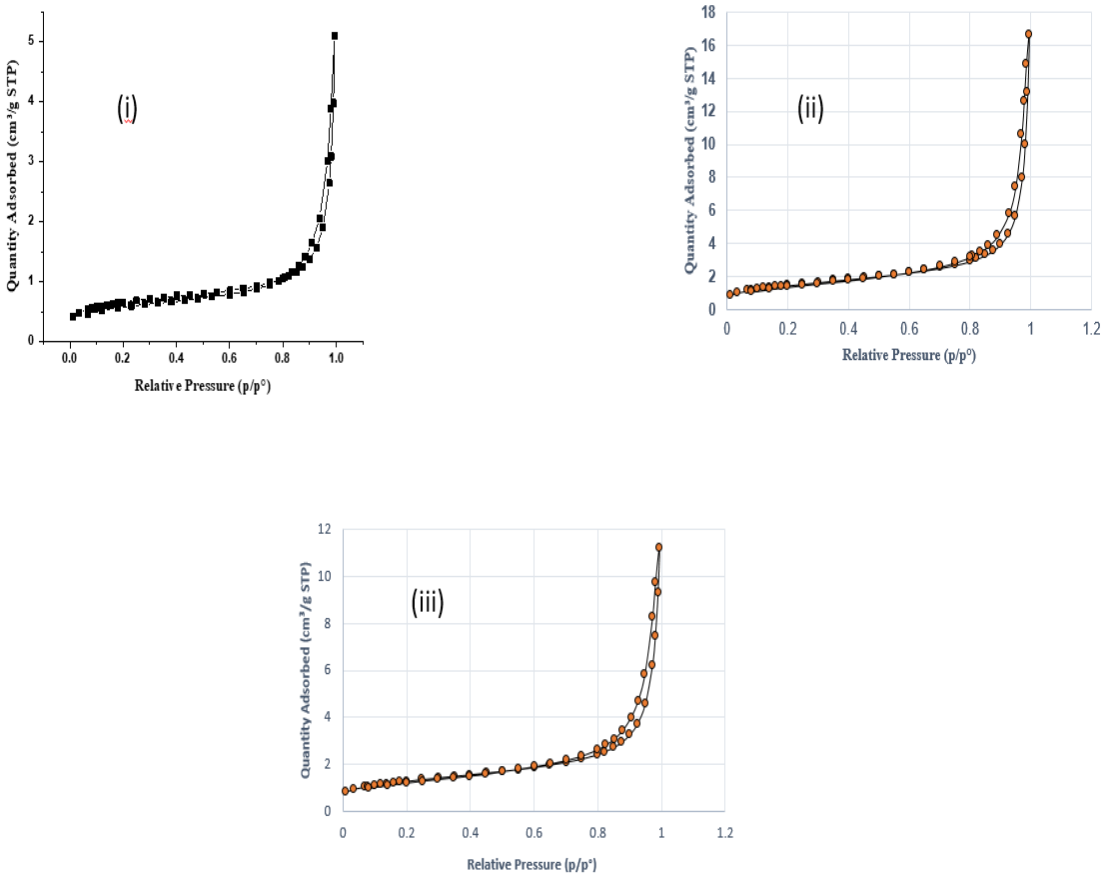

Figure 1: N_2 adsorption-desorption isotherm for (i) Geo-hisi-5wt%(s) (ii) Geo-N-5wt%(s) (iii) Geo-N-1wt%(s) + H_2O

3rd attempt:

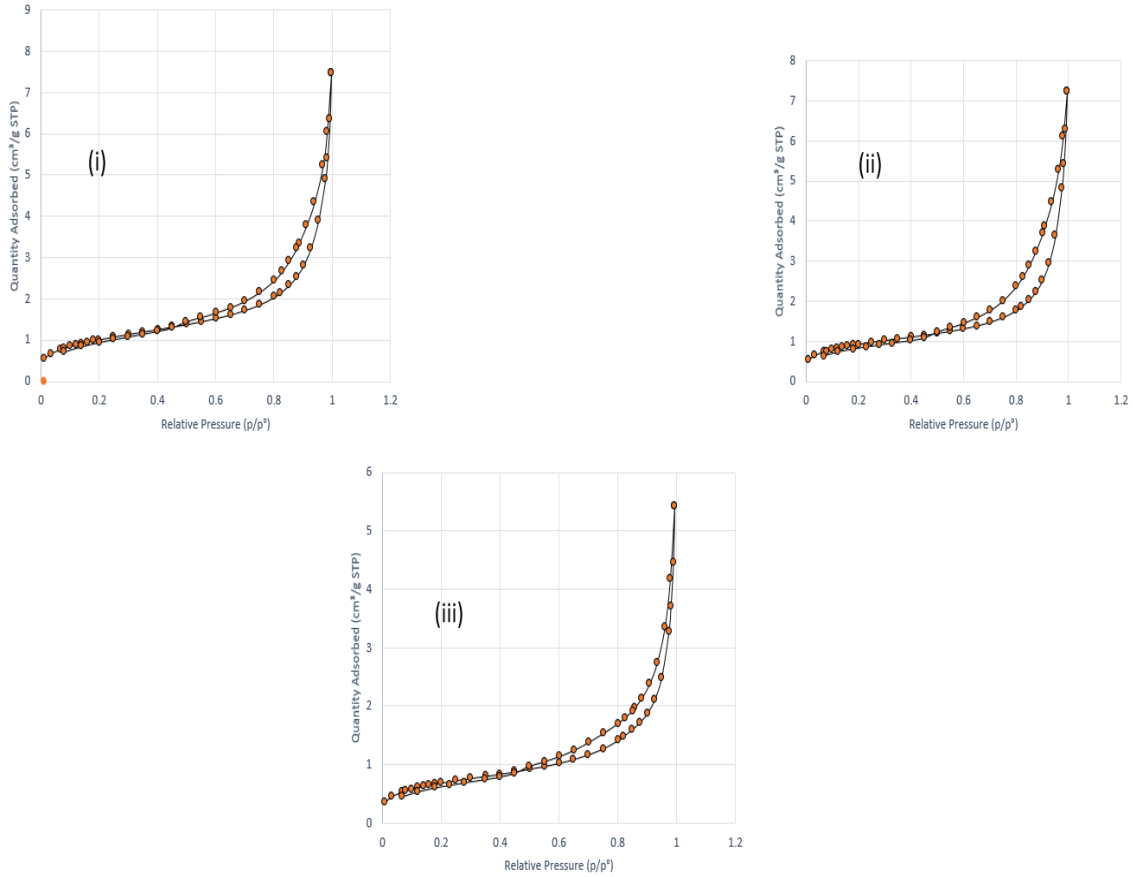

Figure 2: N_2 adsorption-desorption isotherm for (i) Geo-hisi-5wt%(s)– IE (ii) Geo-hisi-10wt%(s)– IE (iii) Geo-hisi-5wt%(s)-FD-IE

4th attempt:

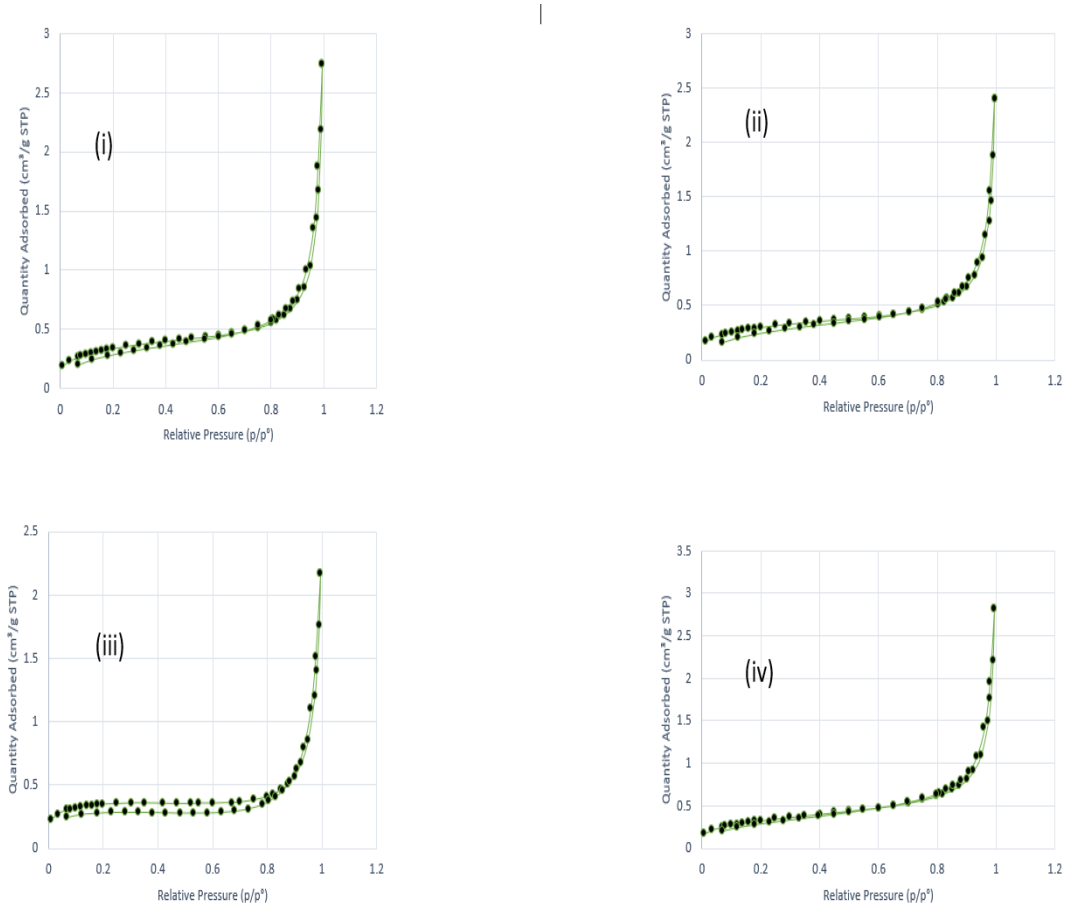

Figure 3: N_2 adsorption-desorption isotherm for (i) Geo-hisi-2.5wt%-FD-IE (ii) Geo-hisi-5wt%-FD-IE (iii) Geo-hisi-10wt%-FD-IE (iv) Geo-hisi-10wt%(s)-IE

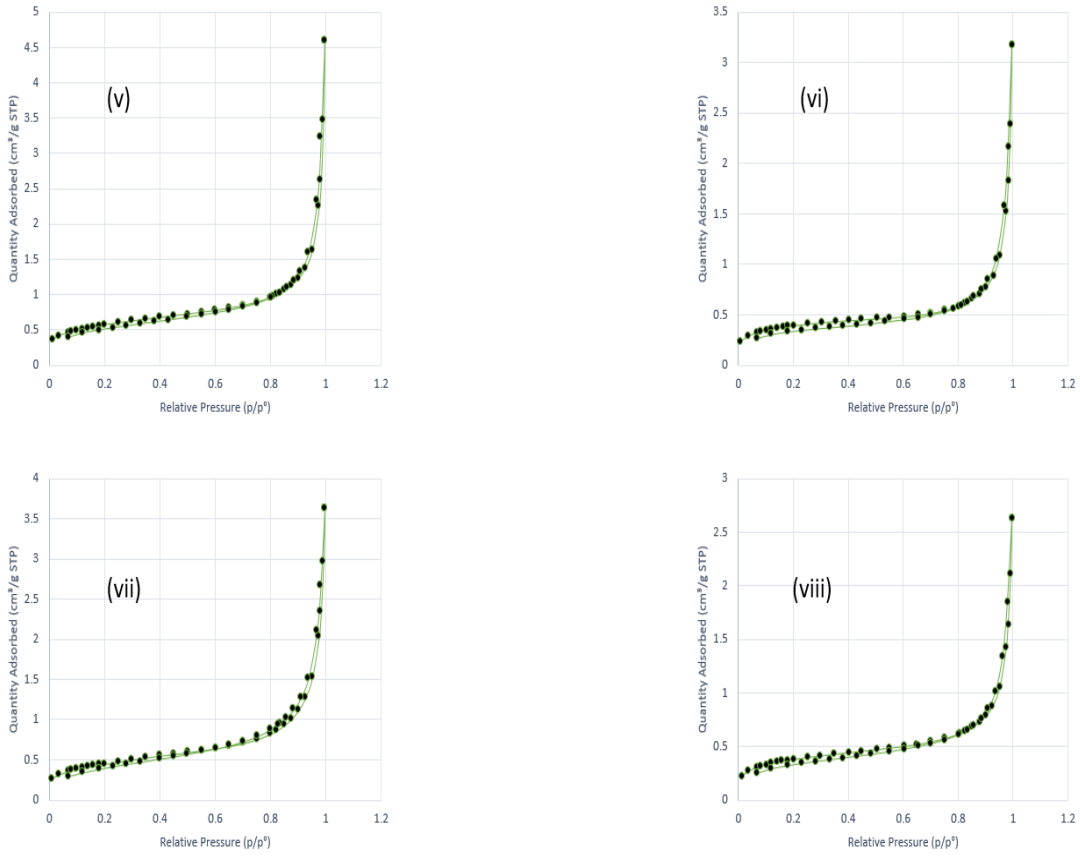

Figure 4: N_2 adsorption-desorption isotherm for (v) Geo-N-2.5wt%-FD-IE (vi) Geo-N-5wt%-FD-IE (vii) Geo-N-10wt%-FD-IE (viii) Geo-N-10wt%(s)-IE

5th attempt:

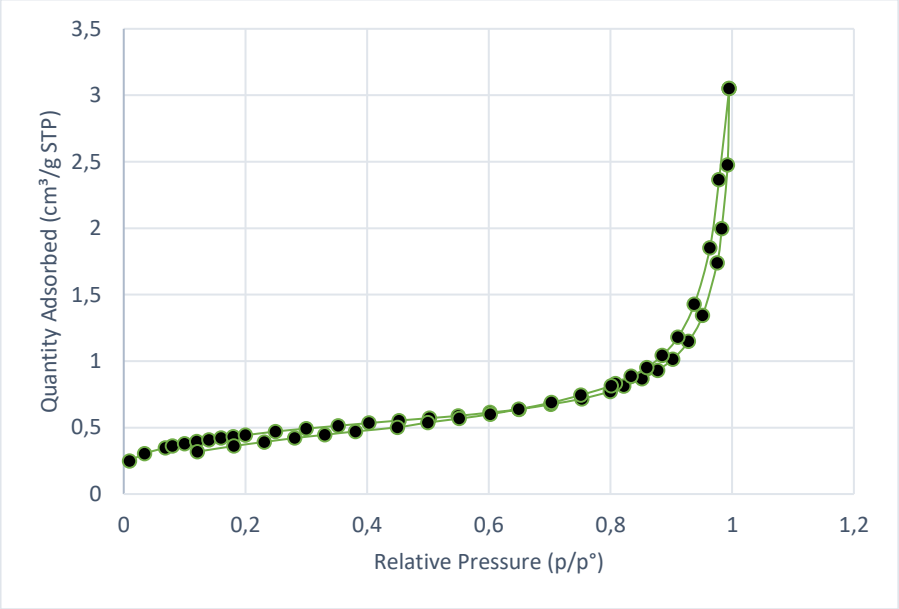

Figure 5: N_2 adsorption-desorption isotherm for Geo-N-2.5wt%-FD-IE

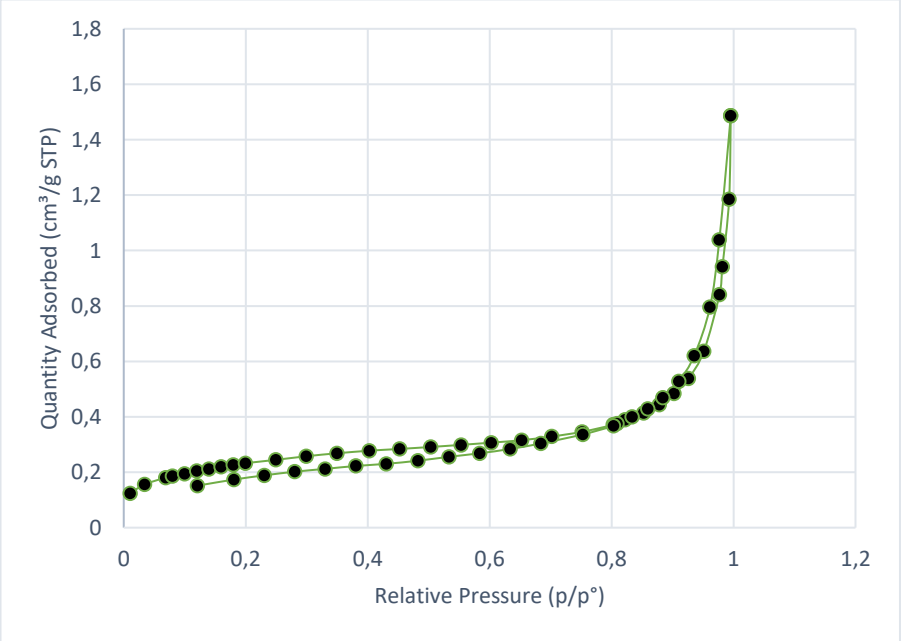

Figure 6: N_2 adsorption-desorption isotherm for Geo-hisi-2.5wt%-FD-IE

6th attempt:

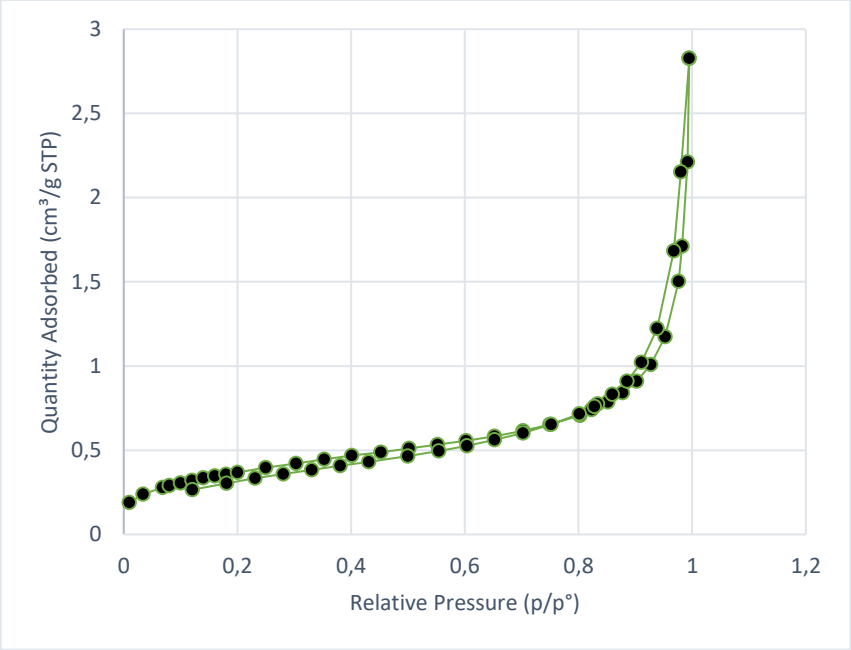

Figure 7: N_2 adsorption-desorption isotherm for Geo-N-10wt%(s)-40

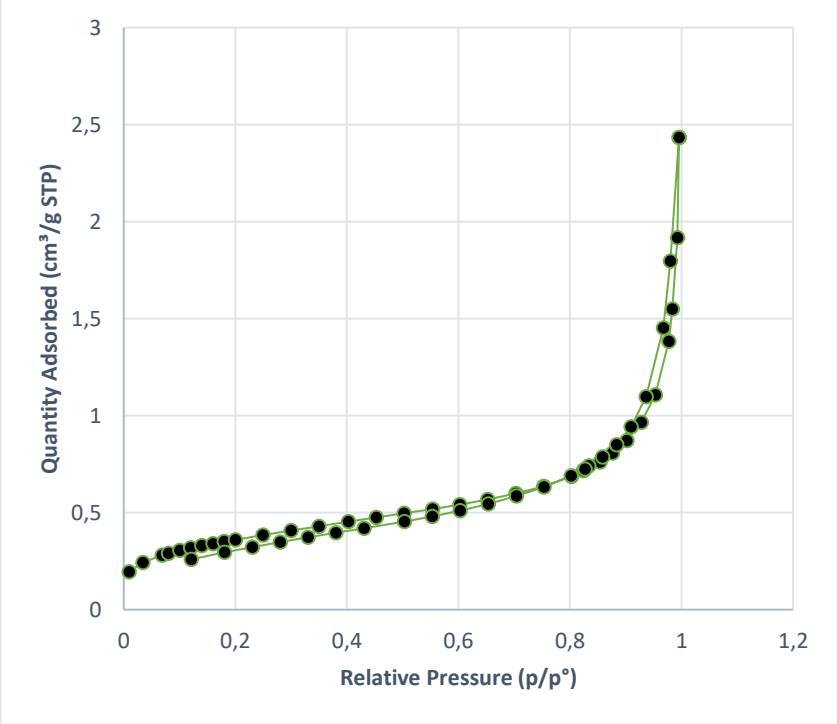

Figure 8: N_2 adsorption-desorption isotherm for Geo-N-10wt%(s)-85

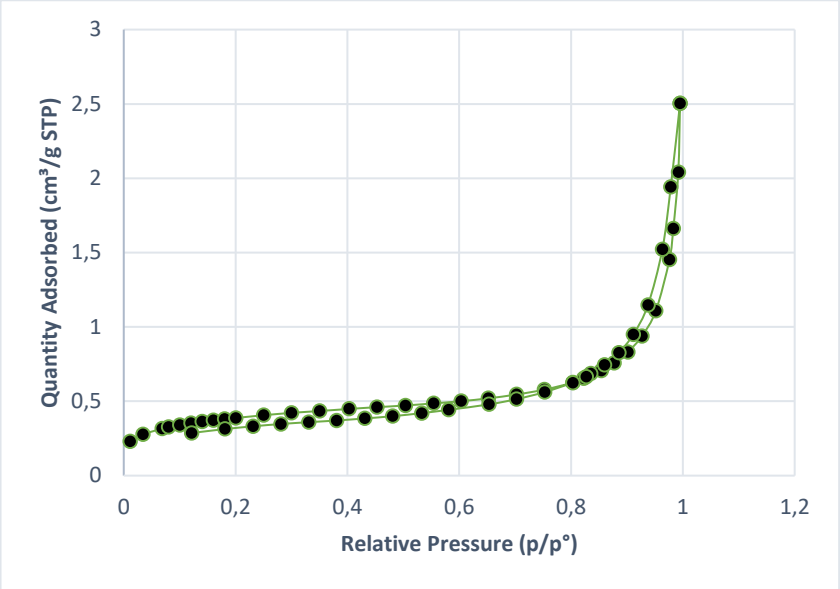

Figure 9: N_2 adsorption-desorption isotherm for Geo-N-10wt%(s)-RT